# Fetus-derived IGF2 matches placental development to fetal demand

Ionel Sandovici[1,2,3,*], Aikaterini Georgopoulou[1,3], Antonia S. Hufnagel[1], Samira N. Schiefer[1], Fátima Santos[3,4], Katharina Hoelle[1], Brian Y.H. Lam[2], Giles S.H. Yeo[2], Keith Burling[2], Jorge López-Tello[3], Moritz Reiterer[5,6], Abigail L. Fowden[3], Graham J. Burton[3], Amanda N. Sferruzzi-Perri[3], Cristina M. Branco[5,6] & Miguel Constância[1,2,3,*]

[1]Department of Obstetrics and Gynaecology and National Institute for Health Research Cambridge Biomedical Research Centre, Cambridge CB2 0SW, United Kingdom

[2]University of Cambridge Metabolic Research Laboratories and MRC Metabolic Diseases Unit, Institute of Metabolic Science, Addenbrookes Hospital, Cambridge CB2 0QQ

[3]Centre for Trophoblast Research, Department of Physiology, Development and Neuroscience, University of Cambridge, Cambridge CB2 3EG, United Kingdom

[4]Epigenetics Programme, Babraham Institute, Cambridge CB22 3AT, United Kingdom

[5]Physiological Laboratory, Department of Physiology, Development and Neuroscience, University of Cambridge, Cambridge CB2 3EG, United Kingdom

[6]Centre for Cancer research and Cell Biology, Queen's University Belfast, Belfast BT9 7AE, United Kingdom

*Correspondence to Ionel Sandovici (is299@cam.ac.uk) or Miguel Constância (jmasmc2@cam.ac.uk)

## Abstract

Growth of a fetus is dependent upon the functional capacity of its placenta, but how the latter is matched to fetal demands is currently unknown. Critically, there is continuous expansion of the feto-placental microvasculature throughout pregnancy, along with morphogenic modifications in the overlying trophoblast epithelium. Here we demonstrate, through fetal and trophoblast specific genetic manipulations in the mouse, that signalling by IGF2 from the feto-placental endothelium and endocrine actions of circulating fetal IGF2 are required. We provide evidence that endothelial and fetal-derived IGF2 plays an important role in trophoblast morphogenesis, acting through *Gcm1* and *Synb*. The effects on placental microvasculature expansion are mediated through IGF2R and angiopoietin-Tie2/TEK signalling. Thus, our study reveals a direct role for IGF2-IGF2R axis on matching fetal demand to placental supply and establishes the principle that hormone-like signals from the fetus play important roles in the control of placental vascularization and trophoblast morphogenesis, findings that have potential clinical implications.

## Main

The mammalian fetus is totally dependent upon the placenta for nutrients and oxygen. Little is known, however, about how placental functional capacity is matched to fetal demands. As gestation progresses, the increase in fetal size requires a higher level of demand for nutrients and consequently a higher level of supply. Depending on the species, the surface area for nutrient exchange increases 5 to 15 fold between mid and late gestation[1]. This remarkable adaptation is likely to occur, at least in part, in response to fetus-derived signals of demand, but this important principle remains untested.

We have proposed that imprinted genes, in particular *Igf2*, play central roles in controlling both the fetal demand for, and the placental supply of, maternal nutrients[2,3,4]. The *Igf2* (insulin-like growth factor 2) gene encodes a small polypeptide that is highly abundant in both fetal tissues and fetal circulation. It is one of the most potent growth factors during intrauterine development, affecting the metabolism, proliferation, survival and differentiation of a wide variety of cell types[5,6,7,8]. In humans, reduced *Igf2* expression contributes to the intra-uterine growth restriction in patients with Silver-Russell syndrome (SRS)[9]. Conversely, bialellic *Igf2* expression caused by loss of *Igf2* imprinting is observed in Beckwith-Wiedemann patients (BWS), a syndrome characterized by somatic overgrowth and increased predisposition to tumours[9]. IGF2 exerts its effects by binding to several IGF/INS receptors (IGF1R, INSR, IGF1/INSR hybrids, IGF2R)[10,11]. IGF2 binds to IGF2R with the highest affinity, which leads to either IGF2 degradation in the lysosomes or signalling via G-proteins[10,12,13].

Here, we apply novel genetic approaches to define the signalling mechanisms of demand to the placenta by creating mouse models with a growth mismatch between the placenta and the fetus, using genetic manipulations of the IGF system. We first show that circulating IGF2 levels increase in late gestation, thus reflecting fetal size and higher demand. Decreasing the demand by lowering IGF2 levels in both the fetus and circulation abolishes the capacity of the placenta to increase the surface area in late gestation; conversely, increased demand by excess fetal IGF2 has the opposite effect. Mechanistically, we show that fetus-derived and circulating IGF2 signalling is essential for the appropriate growth of the fetal-derived vasculature and the underlying trophoblast. These effects are mediated in part by IGF2-IGF2R signalling in the feto-placental vascular endothelium. Our work demonstrates that the interaction of circulating IGF2 and endothelial IGF2 with the trophoblast is essential for matching the placental surface area for nutrient exchange (supply) to the growth rate of fetal tissues (demand).

**Expansion of placental labyrinth coincides with elevated levels of circulating and endothelial IGF2**

The gas and nutrient exchange layer of the mouse placenta (labyrinthine zone – Lz) increased in size with gestational age (Fig. 1a), matching the fetal weight (Fig. 1b). Concomitantly, fetal plasma IGF2 increased approximately two-fold between E16 and E19 (Fig. 1c). At these two developmental stages, we also observed a significant and positive correlation between fetal plasma IGF2 and fetal weights (Fig. 1d). Within the placental Lz, *Igf2* expression was the highest in feto-placental endothelial cells (FPEC) (Fig. 1e) and its mRNA levels increased approximately six-fold between E14 and E19 (Fig. 1f). *Igf2* ranked as the highest expressed gene in FPEC RNA-Seq transcriptome at E16, and several other known imprinted genes[14] ranked in the top one hundred out of approximately 14,000 genes detected (Fig. 1g and Supplementary Table 1). IGF2 protein was also highly expressed in FPEC (Fig. 1h), and significantly higher than in the surrounding trophoblast cells (Fig. 1i).

**Fetal and endothelial IGF2 control placental labyrinthine expansion**

To explore whether fetus-derived IGF2 plays a direct role in placental development, we first used a conditional allele ($Igf2^{+/fl}$) to delete *Igf2* in the epiblast lineage using the $Meox2^{Cre}$ line[15] (Fig. 2a and Extended Data Fig. 1). The deletion of *Igf2* from embryonic organs and FPEC, but not extra-embryonic tissues, led to placental growth restriction from E14 onwards (Fig. 2b). Stereological analyses indicated that only the placental compartments containing embryonic-derived structures (i.e. Lz and the chorionic plate – Cp) were smaller in the $Meox2^{Cre/+}$; $Igf2^{+/fl}$ mutants (referred subsequently as $Igf2^{EpiKO}$) (Fig. 2c). The continuous expansion of the Lz, measured as volume increase, that occurs in late gestation between E14 and E19 was severely compromised in mutants (Fig. 2c). The overall volume, surface area and total length of fetal capillaries (FC) were normal at E14, but became abnormal from E16 onwards (Fig. 2d and Extended Data Fig. 2a). Notably, all other components of placental Lz, not

originating from the embryonic lineage, (i.e. labyrinthine trophoblast – LT, and maternal blood spaces – MBS) were also reduced in volume, to a similar extent as the FC (Fig. 2d). These findings provide evidence for a role of fetus-derived IGF2 on the expansion of placental Lz in late gestation.

IGF2 is highly expressed in FPEC as previously shown in Fig. 1e-i. Therefore, we next tested whether endothelial-derived IGF2 plays a role in placental development. *Igf2* deletion in the fetal endothelium, including FPEC, using the *Tek*$^{Cre}$ line[16] (Fig. 2e and Extended Data Fig. 3) led to a moderate but significant fetal and placental growth restriction, evident from E16 onwards (Fig. 2f). Mutant *Tek*$^{Cre/+}$; *Igf2*$^{+/fl}$ (referred subsequently as *Igf2*$^{ECKO}$) placentae had reduced volumes of Cp and Lz at both E16 and E19 (Fig 2g), but less striking when compared to *Igf2*$^{EpiKO}$ mutants (Fig. 2c). Within the Lz, the LT was reduced at both E16 and E19, while the MBS and FC were comparable to controls at E16, but significantly reduced at E19 (Fig. 2h and Extended Data Fig. 2b).

We conclude that the 'small' labyrinthine phenotype observed in *Igf2*$^{EpiKO}$ mutants is more severe than in *Igf2*$^{ECKO}$ mutants, which suggests that full placental Lz expansion in late gestation requires both fetus-derived and endothelial-derived IGF2.

**Fetus-derived IGF2 is essential for placental morphogenesis and microvasculature expansion**

To uncover the molecular mechanisms responsible for the placental Lz expansion, we first performed microarray analysis in micro-dissected Lz samples from E19 *Igf2*$^{EpiKO}$ mutants and controls. Differentially expressed genes (DEG) were enriched in genes implicated in vasculature development and immune responses (Fig. 3a and Extended Data Fig. 4a,b). We identified a classic molecular signature of impaired angiogenesis – reduced angiopoietin-Tie2/TEK signalling[17] (Fig. 3b and Supplementary Table 2). Lower levels of *Angpt1* and *Tek*, and increased expression of *Angpt2* were validated by qRT-PCR in an independent set of biological samples in late gestation (Fig. 3b). Consistent with the well-established roles of the angiopoietin-Tie2/TEK signalling in the control of endothelial cell survival and proliferation[17], placental TUNEL staining revealed a six-fold increase in apoptotic cell frequency in mutants at E16, specifically in the Lz (Fig. 3c). CD31-stained (marking endothelial cells) or methylene blue-stained resin sections revealed the presence of feto-placental capillaries lacking endothelial cells, or obstructed and thrombotic capillaries surrounded by highly disorganized and fragmented endothelial cells (Fig. 3d). These observations indicate that a large proportion of the apoptotic cells are FPEC. Furthermore, endothelial cell proliferation measured by flow cytometry was significantly reduced at E16 (Fig. 3e and Extended Data Fig. 4c), and this finding was confirmed by immunofluorescence (Extended Data Fig. 4d).

In addition to vascular pathways, the expression microarrays also identified transcriptional upregulation of genes related to immune responses and leukocyte migration (Fig. 3a). Among these was *Adgre1*, a gene that encodes the glycoprotein F4/80, a highly specific cell-surface marker for murine macrophages[18]. The up-regulation of *Adgre1* was confirmed by qRT-PCR in placental Lz also at E16–(Fig. 3f). Immunostaining for F4/80 showed that the total number of macrophages in Lz was significantly higher in mutants than controls (Fig. 3f). Additionally, clusters of macrophages surrounding feto-placental capillaries were found exclusively in mutants (Fig. 3g). Next, we assessed the impact of the described increased cell death, reduced cell proliferation and macrophage infiltration, on capillary remodelling across gestation by CD31 immunostaining. The density of FC was dramatically reduced at E16 and E19, suggestive of a disproportionate loss of FPEC (Fig. 3h).

Importantly, the array data indicated downregulation of key genes involved in syncytiotrophoblast differentiation (*i.e. Gcm1* and *Synb* – which are expressed specifically in layer II of the syncytiotrophoblast, SynT-II, which is closest to FC; see Supplementary Table 2). To validate these

observations, we performed qRT-PCR for, and confirmed significant transcriptional reductions of, SynT-II-specific genes[19,20] *Gcm1*, *Synb* and *Slc16a3* (Fig. 3i). However, only the SynT-I specific[19,20,21] gene *Slc16a1* was modestly down-regulated, but not *Ly6e* and *Syna* (Extended Data Fig. 4e).

Together, our data show that lack of fetus-derived IGF2 triggers dysregulation of angiopoietin-Tie2/TEK signalling in late gestation, with consequent reduced FPEC proliferation and excessive cell death with associated placental macrophage infiltration. It also highlights that fetus-derived IGF2 supports normal development of the trophoblast cells, particularly the SynT-II layer, in a paracrine/endocrine manner, with a knock-on effect on the development of maternal blood spaces.

**Endocrine IGF2 is a fetus-derived signal that matches placental supply to fetal demand**

To provide further insights into the roles of fetus-derived IGF2 in matching supply to fetal demand we analysed five genetic models with either deletion of *Igf2* in fetal tissues, endothelium, trophoblast or ubiquitously, or overexpression of *Igf2* in fetal tissues (Fig. 4). For these models we used flow cytometry to count FPEC (defined as $CD31^+/CD41^-$ cells[22]) and measured labyrinthine weight and circulating IGF2 levels. In $Igf2^{EpiKO}$ mutants, as expected from the immunostainings shown in Fig. 3h, we observed a severe deficit in the total number and the proportion of FPEC at E16 and E19, but normal values at E14 (Fig. 4a). The linear Lz expansion expected with gestational age was not observed in this model, matching the severe reductions in FPEC numbers and circulating IGF2 (Fig. 4a). In contrast, in $Igf2^{ECKO}$ mutants lacking endothelial *Igf2*, circulating levels of IGF2 were only moderately reduced and total numbers of FPEC, but not relative numbers, were only significantly reduced at E19 (Fig. 4b). Lz expansion in this model was only blunted at the end of gestation (Fig. 4b). A deletion of *Igf2* specifically in the trophoblast cells of the placenta using $Cyp19^{Cre}$ ($Igf2^{+/fl}$; $Cyp^{Cre/+}$ referred subsequently as $Igf2^{TrKO}$)[23] (Fig. 4c and Extended Data Fig. 5a-e) did not result in changes in FPEC numbers and circulating IGF2, demonstrating that FPEC expansion is independent of trophoblast-derived IGF2. Consequently, Lz expansion was normal in this model (Fig. 4c). Ubiquitous deletion of *Igf2* in embryo and trophoblast using $CMV^{Cre}$ ($Igf2^{+/fl}$; $CMV^{Cre/+}$ referred subsequently as $Igf2^{UbKO}$)[24] (Fig. 4d and Extended Data Fig. 5f) led to a loss of FPEC similar to that observed in the $Igf2^{EpiKO}$ mutants, further demonstrating that trophoblast-derived IGF2 does not contribute significantly to FPEC expansion. Lz weight was severely reduced from E14, in line with the near complete absence of IGF2 in fetal circulation (Fig. 4d). Conversely, reactivating the transcriptionally silent maternal *Igf2* allele in $H19DMD^{fl/+}$; $Meox2^{+/Cre}$ mutants[25] (referred subsequently as *H19*-$DMD^{EpiKO}$) (Fig. 4e and Extended Data Fig. 5g,h), which led to increased levels of circulating IGF2, was associated with an increase of Lz weight and higher numbers of FPEC at E16 and E19 (Fig. 4e).

Taken together, these results show that IGF2 produced by fetal organs and secreted into the fetal circulation stimulates the expansion of placental Lz, matching FPEC numbers to the fetal demand.

**IGF2 signalling controls expression of FPEC-derived angiogenic factors**

We hypothesised that the interaction of circulating IGF2 and the trophoblast, via FPEC, are key events underlying the feto-placental microvascular remodelling. To establish the molecular signatures of IGF2 effects on FPEC we carried out RNA-Seq analysis on FACS-isolated endothelial cells from E16 placental Lz of $Igf2^{EpiKO}$ mutants and controls (Fig. 5 and Extended Data Fig. 6). Gene ontology (GO) analysis of DEGs showed statistical enrichment of biological processes related to immune responses, cell migration, impaired cell proliferation and angiogenesis, extracellular matrix organization and response to hypoxia (Fig. 5a,b and Supplementary Table 3). We validated representative DEGs using qRT-PCR in independent biological samples, including genes encoding proteins secreted by the endothelial cells into the extracellular space that have known anti-angiogenic effects (*Angpt2*[17], *Adamts1*[26], *Cxcl10*[27],

*Thbs1*[28]), factors implicated in cell migration and response to hypoxia (*Edn1*[29]), an interferon-response gene (Iigp1[30]), an inhibitor of cell proliferation (*Cdkn1a*[31]) and a regulator of embryonic vascular development (*Hey2*[32]) (Fig. 5c). Next, we searched for transcription factor (TF) binding motifs enriched within the promoters of all DEGs. This analysis identified significant enrichments for binding sites of four TF encoded by DEGs – KLF4, EGR1, IRF7 and HEY2 (Fig. 5d and Supplementary Table 3). Significantly, the four TFs control the expression of several proteins involved in angiogenesis (labelled with * in Fig. 5e and further presented in Supplementary Table 4), some of which are secreted by the endothelial cells into the extracellular space (Supplementary Table 4). This analysis also highlighted several chemokines that were up-regulated in FPEC (such as CCL2[33] and IL15[34]) that are likely involved in attracting and modulating the activity of macrophages that surround the feto-placental capillaries (as shown in Fig. 3g). Thus, we established that IGF2 signalling is necessary for proliferation and survival of FPEC and modulates their angiogenic properties.

**IGF2 signalling on FPEC is independent of IGF1R and is mediated by IGF2R *in vitro* and *in vivo***

To further investigate the role of IGF2 in fetal capillary remodelling and identify the receptors that might mediate its effects on endothelial cells, we isolated primary FPEC from E16 wild-type placental Lz and cultured them *ex vivo* (Extended Data Fig. 7a-c). Only the type I (*Igf1r*) and type II (*Igf2r*) receptors were expressed in FPEC both *in vivo* and *ex vivo* (Fig. 6a,b and Extended Data Fig. 7d). Exposure of cultured FPEC, which express low levels of *Igf2*, to exogenous IGF2 significantly increased their ability to form capillary-like tube structures when seeded on matrigel (Extended Data Fig. 7e and Fig. 6c), demonstrating that IGF2 exerts direct angiogenic effects on FPEC. We also exposed cultured FPEC to $IGF2^{Leu27}$, an analogue previously shown to bind to IGF2R with high selectivity[35], which stimulated capillary-like tube formation although to a lesser extent compared to IGF2 (Fig. 6b,c). When FPEC were treated with IGF2 and picropodophyllin (PPP), a small molecule that inhibits phosphorylation of IGF1R without interfering with INSR activity[36], their ability to form capillary-like tube structures was very similar to that of cells treated with IGF2 alone (Fig. 6b,c). Thus, IGF2 exerts direct angiogenic effects on primary FPEC, which are mediated by IGF2R and are independent of IGF1R.

We further confirmed these *in vitro* findings by knocking-out these receptors (IGF1R and IGF2R) *in vivo*. Accordingly, efficient deletion of *Igf1r* from the endothelium ($Igf1r^{ECKO}$) did not have any significant impact on fetal, whole placenta or placental Lz growth kinetics, nor did it alter the total and relative numbers of FPEC/Lz, apart from a slight increase in the percentage of FPEC at E19 (Extended Data Fig. 8a-e). Strikingly, the deletion of *Igf2r* from the endothelium ($Igf2r^{ECKO}$ – Extended Data Fig. 8f,g) resulted in a reduction in the percentage of FPEC/placental Lz at both E16 and E19, further confirmed by a reduced density of $CD31^{+}$ cells by immunofluorescent staining (Fig. (Fig. 6d, e). The total number of FPEC/Lz was also significantly reduced at E16, but became normal at E19 (Fig. 6d), with Lz being overgrown from E16 onwards (Fig. 6f) coincident with an increase in levels of circulating IGF2 in plasma (Fig. 6g). Together, our *in vitro* and *in vivo* experiments demonstrate that IGF2R mediates, at least partially, the signalling actions of IGF2 on FPEC.

## Discussion

The major finding of this study is the demonstration that fetal growth demand signals are major regulators of placental development and function. Although a vast number of genetic pathways have been discovered that are important for the development of different cell types in the placenta and the fetus, there are no functional genetic investigations to date on how the fetus signals demand to

the placenta and how the placenta matches the fetal demands. We tackled these questions with an innovative experimental design, which is based on the manipulation of the growth rate of fetal tissues independent of the placenta, and vice-versa, in the mouse. We used conditional targeting of imprinted genes with well-established growth functions (*Igf2*, *Igf2r*, *H19*) as model systems (importantly, due to imprinting, the mother is phenotypically normal). The analysis of these models of mismatch between supply and demand allowed us to establish a number of key mechanistic principles that regulate the cooperative signalling between the fetus and the placenta and, consequently, the control of maternal resources.

Firstly, we found that circulating IGF2 correlates positively with fetal size in late gestation, reflecting the growth rate of fetal tissues and the demand for nutrients. Mice with a severe decrease in levels of circulating/fetal IGF2, and thus fetal demand, showed a drastic (and disproportionate) loss of feto-placental endothelial cells. This severe placental angiogenesis phenotype was associated with reduced endothelial cell proliferation and increased apoptosis, altered differentiation of the overlying trophoblast and reduced density of maternal blood spaces, ultimately leading to a failure in the expansion of the labyrinthine layer and surface area for nutrient transport. Conversely, increased demand for nutrients caused by bi-allelic *Igf2* expression, which drove higher growth rates, led to 'overexpansion' of the labyrinthine layer. Secondly, we also found that feto-placental endothelial cells are a significant source of IGF2, with levels increasing with gestational age. Endothelial *Igf2*-deficient mice show modest reductions in circulating IGF2 and impaired expansion of the microvasculature and labyrinthine layer, but no disproportionate reduction in number of placental endothelial cells (which is only seen when circulating IGF2 is severely reduced). These findings establish the important principle that hormone-like signals from the fetus, such as IGF2, are required for the normal expansion of the labyrinthine layer and surface area of the placenta.

Based on the experimental evidence provided in this study, we propose a model (Fig. 6h) in which fetus-derived IGF2 is the signal that allows matching placental supply capacity to fetal demand. At the placenta interface, circulating IGF2 directly stimulates endothelial cell proliferation and survival, and capillary branching through IGF2R (as shown *in vivo* and *ex-vivo*). Circulating IGF2 may also directly control the growth and differentiation of the underlying trophoblast, as it can cross (in free form or in binary complexes) the capillary walls or permeate through the fenestrated endothelium[37]. We suggest that the feto-placental endothelium is a large reservoir of IGF2, boosting further IGF2 signalling, and acting in a paracrine and autocrine manner to control the growth and remodelling of fetal capillaries, and trophoblast morphogenesis. Importantly, the effect of IGF2 signalling on feto-placental microvascular remodelling seems specifically driven by fetus-derived IGF2. Accordingly, we did not find any evidence that IGF2 produced by the trophoblast has a direct role on vascularization, being instead required for trophoblast morphogenesis. We therefore suggest that the key role of circulating IGF2 is to provide fetus-derived angiogenic signals to promote the vascular tree expansion in later gestation, in conjunction with local IGF2, derived from the fetal endothelium of the placenta. Mechanistically, the most likely molecular effectors of fetus-derived IGF2 signalling on microvasculature expansion and trophoblast morphogenesis are the angiopoietin-Tie2/TEK signalling and the key trophoblast differentiation genes *Gcm1* and *Synb*, respectively.

Our study has a number of important implications. It provides insights into the complex interplay between trophoblast branching morphogenesis and placental vascularization. To our knowledge, IGF2 is the first example of a hormone-like molecule that signals fetal demand to the placenta by adapting the expansion of feto-placental microvasculature and trophoblast morphogenesis to the embryo size. Matching placental supply to fetal demand also involves IGF2R – the other imprinted member of the IGF family[38]. The imprinting of the IGF system is thus likely to have played a key evolutionary role in

the origins of the expansion of the feto-placental microvasculature and surface area for nutrient transport throughout pregnancy – a fundamental biological process that is observed in all eutherian species[1]. In humans, circulating levels of IGF2 in the umbilical cord progressively increase between 29 weeks of gestation and term, similarly to our findings in the mouse[39]. Additionally, large-for-gestational age and small-for-gestational age babies, have been reported to show increased and reduced levels of IGF2 in the umbilical cord, respectively[40,41]. Moreover, placentae obtained from imprinting growth syndrome patients with disrupted IGF2 signalling are often associated with placentomegaly in BWS cases, due to hypervascularization and hyperplasia[42,43] and small hypoplastic placentas in SRS cases[44], showing striking similarities to our mouse studies. Importantly, most cases of poor placentation in FGR (fetal growth restriction) reported so far were related to placental malperfusion from the maternal side and in response to a perturbed maternal environment[45]. Our findings suggest that poor placentation in humans could be caused by deficient microvasculature expansion due to reduced fetus-derived IGF2 signalling, with important clinical implications.

## Methods

### Mice

Mice were bred, maintained and mated under pathogen-free conditions at the University of Cambridge Phenomics Unit (West Forvie), in accordance with the University of Cambridge Animal Welfare and Ethical Review Body and the United Kingdom Home Office Regulations. The morning of the copulation plug discovery was counted as embryonic day 1 (E1).

The *Igf2*$^{fl/fl}$ mice were generated in our laboratory[46]. *Meox2*$^{Cre}$ mice[15], *Tek*$^{Cre}$ mice[16], *Cyp19*$^{Cre}$ mice[23], *CMV*$^{Cre}$ mice[24] and *Igf1r*$^{fl/fl}$ mice[47] were imported from the Jackson Laboratory (Maine, USA). *Meox2*$^{Cre}$ is active starting at E5 in the epiblast, which gives rise to the entire embryo proper and FPEC[15]. *Tek*$^{Cre}$ (also known as *Tie2*$^{Cre}$) activity starts at E7.5 in the endothelial cell lineage, including FPEC[16]. *Cyp19*$^{Cre}$ is active from E6.5 in the early diploid trophoblast cells that give rise to spongiotrophoblast, giant cells, and labyrinthine trophoblast cells[23]. *CMV*$^{Cre}$ activity starts soon after fertilization and induces ubiquitous deletion of floxed alleles in all tissues, including the germline[24]. *Rosa26* $^{fl}$STOP$^{fl}$YFP mice[48] were kindly provided by Dr. Martin Turner (The Babraham Institute, Cambridge), Ai9(RCL-tdT) mice[49] by Prof. William Colledge (University of Cambridge), *H19*-DMD$^{fl/fl}$ mice[25] and *Igf2r*$^{fl/fl}$ mice[50] by Prof. Bass Hassan (University of Oxford).

All strains were bred into an inbred C57BL/6J genetic background for >10 generations. For all crosses, the parent transmitting the floxed allele was also homozygous for the *Rosa26* $^{fl}$STOP$^{fl}$YFP allele. Thus, YFP expression provided an internal control for efficiency of Cre deletion (see Extended Data Fig. 1,3,5,8). Genotyping was performed by standard PCR using DNA extracted from ear biopsies (adult mice) or tail DNA (fetuses). PCR was performed using the Red Taq Ready PCR system (Sigma) (see list of primers in Supplementary Table 5), followed by separation of PCR amplicons by agarose gel electrophoresis.

### Plasma IGF2 measurements

IGF2 measurements were performed with the Mouse IGF-II DuoSet ELISA kit (R&D Systems – DY792), using an assay adapted for the MesoScale Discovery electrochemiluminescence immunoassay platform (MSD). Briefly, MSD standard-bind microtitre plates were first coated with 30µl capture antibody (Rat Anti-Mouse IGF-II, R&D Systems – 840962) diluted to 7.2 µg/ml in PBS, sealed, and incubated overnight at 4°C. After three washes with MSD wash (0.1% Tween 20 in PBS), the plates

were loaded with 20µl ELISA Diluent RD5-38 per well, plus 10µl standard or plasma (diluted 50 fold in RIPA buffer, Sigma – R0278). The plates were then sealed and incubated for two hours at room temperature on a plate shaker. After three washes with MSD wash, the wells were plated with 25µl detection antibody (Biotinylated Goat Anti-Mouse IGF-II, R&D Systems – 840963), diluted to 0.72 µg/ml in PBS, sealed, and incubated for one hour at room temperature on a plate shaker. Following three additional washes with MSD wash, the wells were plated with 25µl MesoScale Discovery Streptavidin Sulpho-TAG, diluted 1:1000 in the MSD Diluent 100, sealed and incubated for 30 minutes at room temperature on a plate shaker. After three final washes with MSD wash, the wells were plated with 150µl of MSD Read Buffer T (1x) and the reading was performed on the MSD s600 analyser. Each sample was measured in duplicate and the results were calculated against the standard curve, using the MSD Workbench Software.

### *Igf2* mRNA *in situ* hybridization

*In situ* hybridization was performed as described[51], with minor modifications. Briefly, a region of 415bp spanning *Igf2* coding exons 4-6 was PCR amplified using primers: 5'-CACGCTTCAGTTTGTCTGTTCG-3' and 5'-GCTGGACATCTCCGAAGAGG-3' and E14 placental cDNA as template. The PCR amplicon was cloned into a pCR2.1-TOPO plasmid (ThermoFisher Scientific – K450002). Sense (S) and antisense (AS) RNA probes were generated and labelled with Digoxigenin (DIG) by *in vitro* reverse transcription, according to manufacturer's instructions (Roche). E14 fetuses and placentae were collected in ice-cold PBS and fixed overnight in 4% paraformaldehyde in 0.1% diethylpyrocarbonate (DEPC)-PBS at 4°C. Tissues were then dehydrated and embedded in paraffin, using RNase-free conditions. Tissue sections (7µm thick) mounted on polysine slides (VWR) were de-waxed, rehydrated in PBS, post-fixed in 4% paraformaldehyde for 10 minutes, digested with proteinase K (30µg/ml) for 10 min at room temperature, acetylated for 10 minutes (acetic anhydride, 0.25%) and hybridized overnight at 65°C in a humidified chamber with DIG-labeled probes diluted in hybridization buffer. Two 65°C post-hybridization washes (1×SSC, 50% formamide, 0.1% tween-20) followed by two room temperature washes in 1×MABT were followed by 30 minutes RNAse treatment. Sections were blocked for 1 hour in 1×MABT, 2% blocking reagent (Roche), 20% heat-inactivated goat serum and then incubated overnight with anti-DIG antibody (Roche; 1:2,500 dilution) at 4°C. After 4x20 min washes in 1×MABT, slides were rinsed in 1×NTMT and incubated with NBT/BCIP mix in NTMT buffer, according to manufacturer's instructions (Promega). Slides were counterstained with nuclear fast red (Sigma), dehydrated, cleared in xylene and mounted in DPX mounting medium (Sigma). Pictures were taken with an Olympus DP71 bright-field microscope fitted with a camera.

### Western blot analysis

Tissues were lysed in ~10µl/mg tissue RIPA buffer (Sigma – R0278), then the lysates were spun at 3,000 RPM and 4°C for 15 minutes. The supernatants were transferred into new tubes and protein concentrations were quantified using the Pierce BCA Assay Protein kit (Thermo Scientific – 23225). 60µg total protein were mixed with SDS gel loading buffer, then denatured at 70°C for 10 minutes and loaded into 12-well NuPAGE® Novex® 4-12% Bis-Tris precast gels. The pre-stained Novex Sharp protein standard (Invitrogen – LC5800) was used as protein marker. After electrophoresis for 40 minutes at 200V and 4°C, the proteins were transferred onto nitrocellulose membranes, using the iBlot® Transfer Stacks (Invitrogen IB 3010-01) and the iBlot® Gel Transfer Device set for 7 minutes at 20V. Blocking was performed for one hour at 4°C in 5% semi-skimmed milk (Marvel) dissolved in TBS-T. The membranes were then incubated overnight at 4°C with the primary antibody dissolved in 0.5% milk in TBS-T (goat anti-human IGF2, 1:1,000, R&D AF292-NA or goat anti-mouse SOD1, 1:50,000, R&D AF3787). After 2x10 minutes washes with milliQ water and 2x10 minutes washes with TBS-T, the blots were incubated for one hour at room temperature with the secondary antibody dissolved in TBS-T

containing 3% semi-skimmed milk (rabbit anti-goat IgG-HRP, 1:2,500, Santa Cruz sc-2768). The blots were then washed as above, exposed to substrate (Clarity ECL Western Blotting Substrate, Biorad) for 5 minutes and imaged with the Biorad GelDoc system. Stripping of antibodies was carried out using a stripping buffer (ThermoFisher – 21059) for 15 minutes at room temperature. The band intensities were quantified using the ImageLab software (Biorad) and expressed as IGF2/SOD1 ratios.

**Placenta stereology**

Placenta stereology analyses were performed as described[52] in placentae (n=5–7) collected from three litters at each developmental stage. Briefly, the placentae were weighted, then halved and each half placenta weighted again. A half was fixed in 4% paraformaldehyde in PBS at 4°C overnight, then dehydrated and embedded in paraffin wax. The paraffin blocks were exhaustively sectioned using a microtome at 7µm thickness. Placental sections spaced 140 µm apart were hematoxylin-eosin stained and stereological measurements of placental layers were done using the NewCAST system (Visiopharm, Hoersholm, Denmark), using the point counting method[52].

The corresponding placental halves were fixed for 6 hours with 4% glutaraldehyde in 0.1 M PIPES buffer, washed with 0.1 M PIPES buffer, and treated with 1% osmium tetroxide. The samples were then resin-embedded and 1µm thick sections, obtained close to the placental midline, were stained with methylene blue. Analysis of Lz components was done using the NewCAST system (Visiopharm) with meander sampling of ~25% of the Lz area.

**Immunostainings**

Immunohistochemistry or immunofluorescence conditions are listed in Supplementary Table 6. TUNEL staining was performed using the In Situ Cell Death Detection Kit, TMR red (Sigma – 012156792910), according to manufacturer's protocol. EdU staining was done with the Click-iT® EdU Alexa Fluor 488 Imaging Kit (Invitrogen – C10337), according to manufacturer's instructions. For all immunofluorescence stains, DAPI (Sigma – D9542) was used to label the nuclei. For all immunohistochemistry, images were taken with an Olympus DP71 bright-field microscope. Immunofluorescence image acquisition was performed using a LSM510 Meta confocal laser scanning microscope (Carl Zeiss, Jena, Germany) and the ZEN 2009 software. Fluorescence semi-quantification analysis was performed using Volocity 6.3 (Improvision). Counting of $TUNEL^+$ and $F4/80^+$ cells was performed using HALO image analysis software (PerkinElmer).

**qRT-PCR analysis**

Total RNA was extracted using RNeasy Plus Kits (Qiagen – 74134 and 74034). RNA concentration was measured by NanoDrop (Thermo Scientific) and quality was assessed in agarose gels. RNA extracted from FACS isolated cells was quantified and assessed for quality using the RNA 6000 Pico Kit (Agilent – 5067-1513) and an Agilent 2100 Bioanalyzer. Reverse transcription was performed using the RevertAid RT Reverse Transcription Kit (ThermoFisher – K1622). qRT-PCR was performed with the SYBR Green JumpStart Taq Ready Mix (Sigma – S4438) and custom-made primers (Supplementary Table 7) using an ABI Prism 7900 system (Applied Biosystems). For gene expression normalization, we used four housekeeping genes (*Gapdh*, *Sdha*, *Pmm1*, *Ppia*). Levels of expression were calculated using the $2^{-\Delta\Delta Ct}$ method[53].

**Expression microarray analysis**

Total RNA was extracted from E19 male placental Lz using RNeasy Midi Kits (Qiagen – 75144) and quantity and quality were verified using RNA 6000 Nano Kit (Agilent – 5067-1511) and an Agilent 2100 Bioanalyzer. Only RNA samples with RNA integrity numbers (RIN) >9.0 were used. Array profiling was

performed using the Mouse Gene 1.0 ST Array (Affymetrix) and the analysis of the data was performed using GeneSpring GX 12.1 (Agilent, Santa Clara, CA, USA), with two algorithms: RMA (Robust Multiarray Average) and PLIER (Probe Logarithmic Intensity Error). Only genes with $\log_2$ fold change > 0.3 predicted by both algorithms were listed as DEGs. Pathway analysis was performed using Ingenuity Pathway Analysis (version 2012).

**Flow cytometry analysis of FPEC**

Placental labyrinthine layers were micro-dissected in ice-cold PBS. Tissue dissociation into single cells was achieved by digestion at 37°C for 45 minutes with a 0.1% collagenase P solution, aided by mechanical dissociation with needles of decreasing diameter. The cells were then passed through 70-µm cell strainers and washed once in ice-cold PBS + 0.1% BSA. Erythrocytes were lysed using the RBC lysis buffer (BioLegend – 420301). Pelleted cells were then re-suspended in 100µl staining buffer (BioLegend – 420201), counted using the Cedex XS Analyser (Roche) and diluted at 1,000 cells/µl. Blocking of Fc receptors was performed by incubation at 4°C for 20 minutes with an unlabelled anti-CD16/32 (1 µg/million cells; BioLegend – 101320). The cells were then incubated for one hour at 4°C in the dark with a 1:1 mix of anti-mouse CD41 (labelled with Phycoerythrin, PE) (BioLegend – 133906; 0.25 µg per million cells) and anti-mouse CD31 (labelled with AF647) (BioLegend – 102516; 0.25 µg per million cells) in 200µl staining buffer. Stained cells were washed twice in 1ml staining buffer, re-suspended in PBS containing a viability marker (7AAD – 7-Aminoactinomycin, Invitrogen – A1310), filtered again through 70-µm cell strainers and incubated on ice for 5 minutes. Flow cytometry analysis was performed with a BD FACSCantoII machine (BD Biosciences) and 100,000 events were recorded for each sample. FSC files were analysed with the FlowJo_V10 software, using single-cell discrimination and gating based on single-stained controls. FPEC were identified as $7AAD^-$ /$CD31^+$/$CD41^-$ cells.

**Flow cytometry analysis of FPEC proliferation**

Pregnant females received intraperitoneal (i.p.) injections with 50µg of 5-ethynyl-2'-deoxyuridine (EdU)/g body weight, 16 hours prior to tissue collection. Placental Lz dissociation into single cells was performed as above. Cells re-suspended at a concentration of 1000 cells/µl were incubated for 30 minutes at 4°C with 1 µl Red LIVE/DEAD Fixable Dead Cell Stain (ThermoFisher – L23102). After one wash in PBS, the cells were pre-incubated for 20 minutes at 4°C in the dark with unlabelled anti-CD16/32 (BioLegend – 101320, 1 µg/million cells), then for 1 hour at 4°C in the dark with a 1:1 mix of anti-mouse CD41 (labelled with BV421, BioLegend – 133911; 0.25 µg per million cells) and anti-mouse CD31 (labelled with AF647) (BioLegend – 102516; 0.25 µg per million cells) in staining buffer. After two washes with staining buffer, the cells were stained using the Click-iT EdU Alexa Fluor 488 Flow Cytometry Assay Kit (ThermoFisher – C10420), according to manufacturer's instructions. Flow cytometry analysis was performed using a BD LSRFortessa cell analyser (BD Biosciences). FSC files were analysed with the FlowJo_V10 software, using single-cell discrimination and gating based on single-stained controls. Proliferating FPEC were identified as viable $EdU^+$/$CD31^+$/$CD41^-$ cells.

**FPEC isolation by FACS**

For sorting, single cell preparation and staining for FPEC markers was performed as above. FACS was done using an Aria-Fusion cell sorter (BD Bioscience), with exclusion of cell duplets and dying cells ($7AAD^+$). Cell fractions (endothelial and non-endothelial cells) were then spun at 3,000 RPM and 4°C for 3 min, the excess of sorting liquid was removed and cell pellets were flash frozen in liquid $N_2$ and stored at -80°C until used for RNA extraction.

**Primary FPEC isolation, culture and tube formation assay**

Primary FPEC were isolated as previously described[54] and adapted here to placental Lz (E16). Briefly, placental labyrinthine layers were micro-dissected on ice in RPMI containing 1% penicillin/streptomycin. All samples from one litter were pooled, minced and digested for 90 minutes at 37°C in 2 mg/ml collagenase type I (Sigma) in HBSS containing 2mM CaCl2, 2mM MgSO4, and 20mM HEPES. The digests were filtered through 70µm nylon cell strainers and washed in HBSS. The cell pellets were then resuspended in PBS containing 0.1% BSA and incubated with anti-CD31-coated magnetic beads for one hour at 4°C. Cells coated with beads were cultured in endothelial cell growth medium consisting of low glucose DMEM:F12 with 1% nonessential aminoacids, 2mM sodium pyruvate, buffered with 20mM HEPES and supplemented with 20% FBS and 75µg/ml endothelial mitogens (Sigma – E2759). The cells were incubated at 37°C in 5% O2 and 5% CO2. After four days, the dead cells were washed and new media was added, additionally supplemented with 20µg/ml Heparin (Sigma). Sub-confluent cells (~80%) at passage one (around 10 days in culture) were washed and then cultured in 5% serum replacement media (Sigma – S0638) for ~40 hours. From each litter we used cells at passage one for treatment with 50 ng/ml IGF2 (dissolved in PBS), 1000 ng/ml IGF2$^{Leu27}$ (dissolved in 10mM HCl), 500nM PPP (dissolved in DMSO) or 500nM PPP + 50 ng/ml IGF2, or appropriate vehicle control. The cells were harvested with Accutase (Sigma) and counted using the ADAM$^{TM}$ Automated cell counter (NanoEnTek Inc) and 3,000 cells were seeded into 15-well Angiogenesis µ-Slides (Ibidi – 81506) preloaded with 10µl matrigel/well (BD Biosciences – 354234). Photographs were taken at 30 min, 4, 6 and 8 hours using an EVOS FL Cell Imaging system (ThermoFisher Scientific). Each experiment was performed on 5-6 litters for every treatment. For each tube formation assay, we used five wells seeded with primary FPEC exposed to the treatment agent with equivalent numbers of the corresponding vehicle. Quantification of tubular network structures was performed using the Angiogenesis Analyzer software in ImageJ[55].

**RNA-sequencing and data analysis**

Total RNA was extracted from sorted FPEC by FACS from E16 male placentae using RNeasy Plus Micro Kits (Qiagen – 74034). Quantity and quality were verified using the RNA 6000 Pico Kit (Agilent – 5067-1513) and an Agilent 2100 Bioanalyzer. Only RNA samples with RNA integrity numbers (RIN) >9.0 were used. Total RNA (2 ng) was whole-transcriptome amplified using the Ovation RNA–Seq System V2 (NuGEN). To prepare the RNA–seq libraries the amplified cDNA (2µg per sample) was fragmented to 200bp using a Bioruptor Sonicator (Diagenode), end repaired and barcoded using the Ovation Rapid DR Library System (NuGEN). The libraries were combined and loaded onto an Illumina HiSeq 2500 system for single-end 50bp sequencing at the Genomics Core Facility, Cambridge Institute, CRUK. The reads were aligned onto the mouse GRCm38 genome using TopHat 2.0.11[56]. Gene abundance and differential expression were determined with Cufflinks 2.2.1[57] and expressed in fragments per kilobase per million mapped reads (FPKM). The cut off for expression was set at ≥1 FPKM. Genes with a linear fold expression change greater than 1.5 and a Benjamini–Hochberg false discovery rate (FDR) <5% were considered differentially expressed.

Functional analysis was performed using DAVID (Database for Annotation, Visualization and Integrated Discovery; v6.8 http://david.abcc.ncifcrf.gov/). Enriched gene ontology (GO) terms with FDR < 5% were considered significant. These terms were then clustered semantically using REViGO (Reduce and Visualize GO)[58], which removes redundancy, and ordered according to the $\log_{10}$ *P* values.

To search for enrichment of TF binding sites at the promoters of DEG, we used EPD (Eukaryotic Promoter Database – https://epd.vital-it.ch/index.php) to retrieve the DNA sequences from 1,000bp upstream to 100bp downstream of the transcriptional start site (TSS). These sequences were then analysed using AME (Analysis of Motif Enrichment v4.12.0 – http://meme-suite.org/tools/ame) by

selecting *Mus musculus* and HOCOMOCO Mouse (v11 FULL) as motif database. Transcriptional network visualization was performed using the Ingenuity Pathway Analysis tool.

**Statistical analysis**

No statistical analysis was used to predetermine sample size. Randomization was not used in our animal studies. Placental stereology and histological EdU analyses were performed blinded to genotype. All statistical analyses were performed using GraphPad Prism 7. Statistical significance between two groups was determined by Mann-Whitney tests or two-tailed unpaired t-tests and statistical significance between multiple groups was performed using one-way ANOVA plus Tukey's multiple comparisons tests or two-way ANOVA plus Sidak's multiple comparisons tests, as appropriate. The numbers of samples used for each experiment are indicated in figure legends.

**Data availability**

Expression microarray and RNA-seq data have been deposited in the Gene Expression Omnibus (GEO) (pending accession codes). Other data and materials are available upon request from the corresponding authors.

**Acknowledgements**

This work was supported by Biotechnology and Biological Sciences Research Council (grant BB/H003312/1 to MC), Medical Research Council (MRC_MC_UU_12012/4 to MC; MRC_MC_UU_12012/5 to the MRC Metabolic Diseases Unit), Centre for Trophoblast Research and the NIHR Cambridge BRC Cell Phenotyping Hub. We thank Nuala Daw, Barbara Villela and Bliss Anderson for technical assistance with the placental stereology analyses, Adrian Wayman and Laura Hunter (West Forvie Phenomics Center) for help with mouse husbandry; Keli Philips and James Warner (Histology Core Facility) for help with preparing tissue samples for histology and F4/80 staining, Gregory Strachan (Imaging Core Facility) for help with TUNEL$^+$ and F4/80$^+$ cells counting using HALO, Marcella Ma (Genomics and Transcriptomics Core) for help with preparing the RNA-Seq libraries and Natalia Savinykh and Esther Perez (NIHR Cambridge BRC Cell Phenotyping Hub) for help with flow cytometry cell sorting.

**Contributions**

IS and AG performed all the *in vivo* experimental work, with contributions from ASH, SNS, FS, KH, JL-T and AS-P. IS, BYHL and GSHY performed bioinformatics analyses. IS, MR and CMB performed the *in vitro* tube formation assays. KB developed and performed the assay for IGF2 measurements in fetal plasma. IS and MC designed the project and GJB, ALF, AS-P and CMB assisted with the experimental design and data analysis/interpretation. IS, GJB and MC wrote the manuscript, with important contributions from ALF, AS-P and CMB. All other authors discussed the results and edited the manuscript. MC managed and supervised all aspects of the study.

**References**

1. Fowden, A.L., Ward, J.W., Wooding, F.P., Forhead, A.J. & Constância, M. Programming placental nutrient transport capacity. *J. Physiol.* **572**, 5–15 (2006).
2. Constância, M. *et al.* Adaptation of nutrient supply to fetal demand in the mouse involves interaction between the Igf2 gene and placental transporter systems. *Proc. Natl. Acad. Sci. USA* **102**, 19219–19224 (2005).

3. Constância, M. *et al.* Placental-specific IGF-II is a major modulator of placental and fetal growth. *Nature* **417**, 945-948 (2002).
4. Angiolini, E. *et al.* Developmental adaptations to increased fetal nutrient demand in mouse genetic models of Igf2-mediated overgrowth. *FASEB J.* **25**, 1737–1745 (2011).
5. DeChiara, T.M., Robertson, E.J. & Efstratiadis, A. Parental imprinting of the mouse insulin-like growth factor II gene. *Cell* **64**, 849–859 (1991).
6. Baker, J., Liu, J.P., Robertson, E.J. & Efstratiadis, A. Role of insulin-like growth factors in embryonic and postnatal growth. *Cell* **75**, 73–82 (1993).
7. Burns, J.L. & Hassan, A.B. Cell survival and proliferation are modified by insulin-like growth factor 2 between days 9 and 10 of mouse gestation. *Development* **128**, 3819–3830 (2001).
8. Gardner, R.L., Squire,S., Zaina, S., Hills, S. & Graham, C.F. Insulin-like growth factor-2 regulation of conceptus composition: effects of the trophectoderm and inner cell mass genotypes in the mouse. *Biol. Reprod.* **60**, 190–195 (1999).
9. Azzi, S., Abi Habib, W. & Netchine, I. Beckwith-Wiedemann and Russell-Silver Syndromes: from new molecular insights to the comprehension of imprinting regulation. *Curr. Opin. Endocrinol. Diabetes Obes.* **21**, 30–38 (2014).
10. Sferruzzi-Perri, A.N., Sandovici, I., Constancia, M. & Fowden, A.L. Placental phenotype and the insulin-like growth factors: resource allocation to fetal growth. *J. Physiol.* **595**, 5057–5093 (2017).
11. Harris, L.K. & Westwood. M. Biology and significance of signalling pathways activated by IGF-II. *Growth Factors* **30**, 1–12 (2012).
12. Okamoto, T. *et al.* A simple structure encodes G protein-activating function of the IGF-II/mannose 6-phosphate receptor. *Cell* **62**, 709–717 (1990).
13. Maeng, Y.S. *et al.* Endothelial progenitor cell homing: prominent role of the IGF2-IGF2R-PLCbeta2 axis. *Blood* **113**, 233–243 (2009).
14. Wei, Y. *et al.* MetaImprint: an information repository of mammalian imprinted genes. *Development* **141**, 2516–2523 (2014).
15. Tallquist, M.D. & Soriano, P. Epiblast-restricted Cre expression in MORE mice: a tool to distinguish embryonic vs. extra-embryonic gene function. *Genesis* **26**, 113–115 (2000).
16. Kisanuki, Y.Y. *et al.* Tie2-Cre transgenic mice: a new model for endothelial cell-lineage analysis in vivo. *Dev. Biol.* **230**, 230–242 (2001).
17. Augustin, H.G., Koh, G.Y., Thurston, G. & Alitalo, K. Control of vascular morphogenesis and homeostasis through the angiopoietin-Tie system. *Nat. Rev. Mol. Cell Biol.* **10**, 165–177 (2009).
18. Austyn, J.M. & Gordon, S. F4/80, a monoclonal antibody directed specifically against the mouse macrophage. *Eur. J. Immunol.* **11**, 805–815 (1981).
19. Rawn, S.M. & Cross, J.C. The evolution, regulation, and function of placenta-specific genes. *Annu. Rev. Cell. Dev. Biol.* **24**, 159–181 (2008).
20. Nagai, A. et al. Cellular expression of the monocarboxylate transporter (MCT) family in the placenta of mice. *Placenta* **31**, 126–133 (2010).
21. Hughes, M., Natale, B.V., Simmons, D.G. & Natale, D.R. Ly6e expression is restricted to syncytiotrophoblast cells of the mouse placenta. *Placenta* **34**, 831–835 (2013).
22. Rhodes, K.E. et al. The emergence of hematopoietic stem cells is initiated in the placental vasculature in the absence of circulation. *Cell Stem Cell* **2**, 252–263 (2008).
23. Wenzel, P.L. & Leone, G. Expression of Cre recombinase in early diploid trophoblast cells of the mouse placenta. *Genesis* **45**, 129–134 (2007).
24. Schwenk, F., Baron, U. & Rajewsky, K. A cre-transgenic mouse strain for the ubiquitous deletion of loxP-flanked gene segments including deletion in germ cells. *Nucleic Acids Res.* **23**, 5080–5081 (1995).
25. Srivastava, M. *et al.* H19 and Igf2 monoallelic expression is regulated in two distinct ways by a shared cis acting regulatory region upstream of H19. *Genes Dev.* **14**, 1186–1195 (2000).

26. Lee, N.V. *et al.* ADAMTS1 mediates the release of antiangiogenic polypeptides from TSP1 and 2. *EMBO J.* **25**, 5270–5283 (2006).
27. Angiolillo, A.L. *et al.* Human interferon-inducible protein 10 is a potent inhibitor of angiogenesis in vivo. *J. Exp. Med.* **182**, 155–162 (1995).
28. Lawler, P.R. & Lawler, J. Molecular basis for the regulation of angiogenesis by thrombospondin-1 and -2. *Cold Spring Harb. Perspect. Med.* **2**, a006627 (2012).
29. Lankhorst, S., Danser, A.H. & van den Meiracker, A.H. Endothelin-1 and antiangiogenesis. *Am. J. Physiol. Regul. Integr. Comp. Physiol.* **310**, R230–R234 (2016).
30. Uthaiah, R.C., Praefcke, G.J., Howard, J.C. & Herrmann, C. IIGP1, an interferon-gamma-inducible 47-kDa GTPase of the mouse, showing cooperative enzymatic activity and GTP-dependent multimerization. *J. Biol. Chem.* **278**, 29336–29343 (2003).
31. Vidal, A. & Koff, A. Cell-cycle inhibitors: three families united by a common cause. *Gene* **247**, 1–15 (2000).
32. Fischer, A., Schumacher, N., Maier, M., Sendtner, M. & Gessler, M. The Notch target genes Hey1 and Hey2 are required for embryonic vascular development. *Genes Dev.* **18**, 901–911(2004).
33. Gregory, J.L. *et al.* Macrophage migration inhibitory factor induces macrophage recruitment via CC chemokine ligand 2. *J. Immunol.* **177**, 8072–8079 (2006).
34. Fehniger, T.A. & Caligiuri, M.A. Interleukin 15: biology and relevance to human disease. *Blood* **97**, 14–32 (2001).
35. Beukers, M.W. *et al.* [Leu27] insulin-like growth factor II is highly selective for the type-II IGF receptor in binding, cross-linking and thymidine incorporation experiments. *Endocrinology* **128**, 1201–1203 (1991).
36. Girnita, A. *et al.* Cyclolignans as inhibitors of the insulin-like growth factor-1 receptor and malignant cell growth. *Cancer Res.* **64**, 236–242 (2004).
37. Bach, L.A. Endothelial cells and the IGF system. *J. Mol. Endocrinol.* **54**, R1–R13 (2015).
38. Constância, M., Kelsey, G. & Reik W. Resourceful imprinting. *Nature* **432**, 53–57 (2004).
39. Gohlke, B.C., Fahnenstich, H., Dame, C. & Albers, N. Longitudinal data for intrauterine levels of fetal IGF-I and IGF-II. *Horm. Res.* **61**, 200–204 (2004).
40. Verhaeghe, J. *et al.* C-peptide, insulin-like growth factors I and II, and insulin-like growth factor binding protein-1 in umbilical cord serum: correlations with birth weight. *Am. J. Obstet. Gynecol.* **169**, 89–97 (1993).
41. Tzschoppe, A. et al. Differential effects of low birthweight and intrauterine growth restriction on umbilical cord blood insulin-like growth factor concentrations. *Clin. Endocrinol. (Oxf).* **83**, 739–745 (2015).
42. Aoki, A. *et al.* Beckwith-Wiedemann syndrome with placental chorangioma due to H19-differentially methylated region hypermethylation: a case report. *J. Obstet. Gynaecol. Res.* **37**, 1872–1876 (2011).
43. Armes, J.E. *et al.* The placenta in Beckwith-Wiedemann syndrome: genotype-phenotype associations, excessive extravillous trophoblast and placental mesenchymal dysplasia. *Pathology* **44**, 519–527 (2012).
44. Yamazawa, K. *et al.* Molecular and clinical findings and their correlations in Silver-Russell syndrome: implications for a positive role of IGF2 in growth determination and differential imprinting regulation of the IGF2-H19 domain in bodies and placentas. *J. Mol. Med.* **86**, 1171–1181 (2008).
45. Mayhew, T.M., Charnock-Jones, D.S. & Kaufmann, P. Aspects of human fetoplacental vasculogenesis and angiogenesis. III. Changes in complicated pregnancies. *Placenta* **25**, 127–139 (2004).
46. Haley, V.L. *et al.* Igf2 pathway dependency of the Trp53 developmental and tumour phenotypes. *EMBO Mol. Med.* **4**, 705–718 (2012).

47. Dietrich, P., Dragatsis, I., Xuan, S., Zeitlin, S. & Efstratiadis, A. Conditional mutagenesis in mice with heat shock promoter-driven cre transgenes. *Mamm. Genome* **11**, 196–205 (2000).
48. Srinivas, S. *et al.* Cre reporter strains produced by targeted insertion of EYFP and ECFP into the ROSA26 locus. *BMC Dev. Biol.* **1**, 4 (2001).
49. Madisen, L. *et al.* A robust and high-throughput Cre reporting and characterization system for the whole mouse brain. *Nat. Neurosci.* **13**, 133–40 (2010).
50. Wylie, A.A. *et al.* Tissue-specific inactivation of murine M6P/IGF2R. *Am. J. Pathol.* **162**, 321–328 (2003).
51. Simmons, D.G., Rawn, S., Davies, A., Hughes, M. & Cross, J.C. Spatial and temporal expression of the 23 murine Prolactin/Placental Lactogen-related genes is not associated with their position in the locus. *BMC Genomics* **9**, 352 (2008).
52. Coan, P.M., Ferguson-Smith, A.C. & Burton, G.J. Developmental dynamics of the definitive mouse placenta assessed by stereology. *Biol. Reprod.* **70**, 1806–1813 (2004).
53. Livak, K.J. & Schmittgen, T.D. Analysis of relative gene expression data using real-time quantitative PCR and the 2(-Delta Delta C(T)) Method. *Methods* **25**, 402–408 (2001).
54. Branco-Price, C. *et al.* Endothelial cell HIF-1α and HIF-2α differentially regulate metastatic success. *Cancer Cell* **21**, 52–65 (2012).
55. Schneider, C.A., Rasband, W.S. & Eliceiri, K.W. NIH Image to ImageJ: 25 years of image analysis. *Nat. Methods* **9**, 671–675 (2012).
56. Kim, D. *et al.* TopHat2: accurate alignment of transcriptomes in the presence of insertions, deletions and gene fusions. *Genome Biol.* **14**, R36 (2013).
57. Trapnell, C. *et al.* Transcript assembly and quantification by RNA-seq reveals unannotated transcripts and isoform switching during cell differentiation. *Nat. Biotechnol.* **28**, 511–515 (2010).
58. Supek, F., Bošnjak, M., Škunca, N. & Šmuc, T. REVIGO summarizes and visualizes long lists of gene ontology terms. *PLoS One* **6**, e21800 (2011).

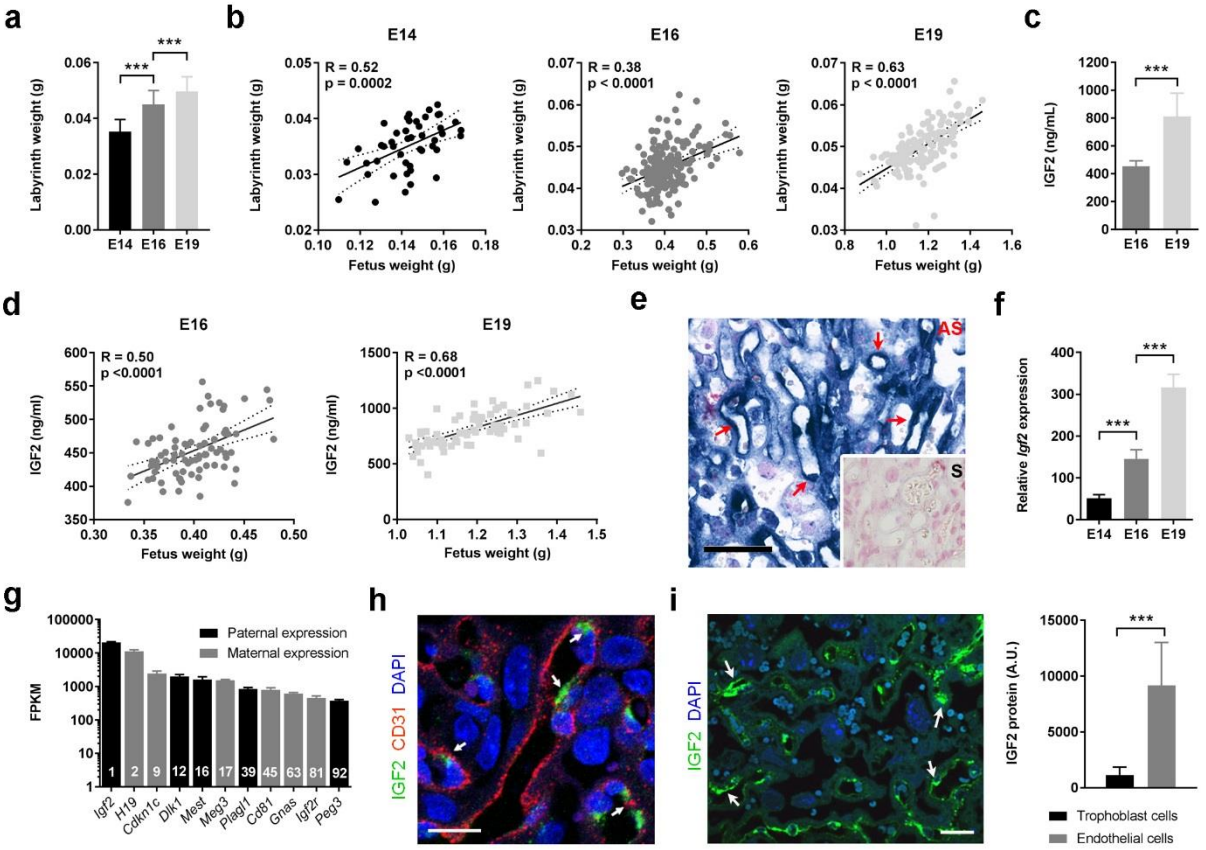


**Figure 1: Placental Lz expansion is associated with increasing levels of circulating and endothelial IGF2.**

**a,** Weights of micro-dissected Lz. **b,** Linear correlation analyses between fetal and placental Lz weights (n=46–189 placentae from n>10 litters per group in **a**, **b**). **c,** Levels of IGF2 (ng/mL) in plasma of wild-type fetuses. **d,** Linear correlation analyses between fetal weights and circulating IGF2 (n=70–79 per group in **c**, **d**). **e,** *Igf2* mRNA *in situ* hybridization (blue) in E14 wild-type placental Lz (red arrows– FPEC; AS – antisense probe; inset with sense probe – S; scale bar is 50µm). **f,** Relative *Igf2* mRNA expression levels measured by qRT-PCR in FPEC from wild-type placental Lz (n=6–7 per group). **g,** Imprinted genes that rank within top 100 expressed genes in E16 wild-type FPEC (FPKM – Fragments Per Kilobase Million; n=4). **h,** Double immunostaining for IGF2 and CD31 in E19 wild-type placenta, demonstrating expression in FPEC. Endothelial cells are very thin and hard to detect except where the cytoplasm is more voluminous around the nucleus, with intense IGF2 stain (white arrows). Transmembrane glycoprotein CD31 immunostaining is in the membrane and largely marks endothelial intercellular junctions (scale bar is 20µm)**. i,** Semi-quantitative measurement of IGF2 protein in FPEC versus trophoblast cells (E19 wild-type placental Lz, n=60 cells per group from two placentae). White arrows – endothelial cells; scale bar is 50µm. Data (**a**, **c**, **f**, **g**, **i**) is presented as averages ± standard deviation (SD); *** *P*<0.001 calculated by one-way ANOVA plus Tukey's multiple comparisons test (**a, f**) or by unpaired *t*-test with Welch's correction (**c**, **i**).

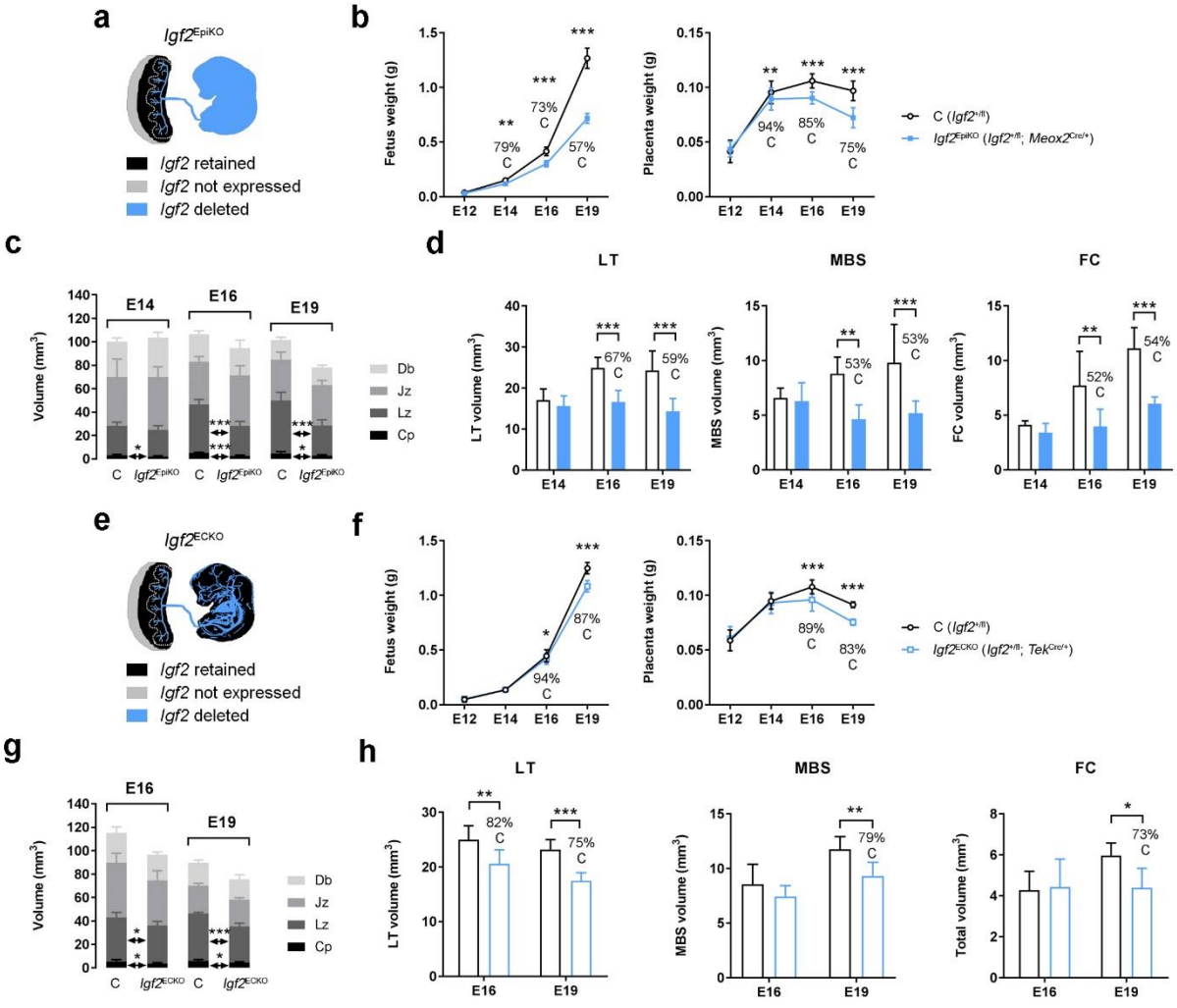


679

680

681 **Figure 2: Deletion of *Igf2* in the epiblast or endothelium impairs placental Lz expansion.**

682 **a,** Schematic of *Igf2* expression in conceptuses with conditional deletion driven by *Meox2*$^{Cre}$. **b,** Fetal
683 and placental growth kinetics (E12: n=10 litters; E14: n=22 litters; E16: n=36 litters; E19: n=34 litters).
684 **c,** Absolute volumes of the placental layers (Db – decidua basalis, Jz – junctional zone, Lz – labyrinthine
685 zone, Cp – chorionic plate), measured by stereology. **d,** Absolute volumes (in mm$^3$) of placental Lz
686 components, measured by stereology (LT – labyrinthine trophoblast, MBS – maternal blood spaces,
687 FC – fetal capillaries) (n=6 per group). **e,** Schematic of *Igf2* expression in conceptuses with conditional
688 deletion driven by *Tek*$^{Cre}$. **f,** Fetal and placental growth kinetics (E12: n=4 litters; E14: n=8 litters; E16:
689 n=13 litters; E19: n=7 litters). **g,** Absolute volumes of the placental layers measured by stereology
690 (n=5–7 per group). **h,** Absolute volumes (in mm$^3$) of placental Lz components, measured by stereology.
691 For all graphs data is shown as averages; error bars represent SD; * *P*<0.05; ** *P*<0.01; *** *P*<0.001
692 calculated by two-way ANOVA plus Sidak's multiple comparisons tests (**b**, **d**, **f**, **h**) or unpaired t tests
693 (**d**, **g**).

694

695

696

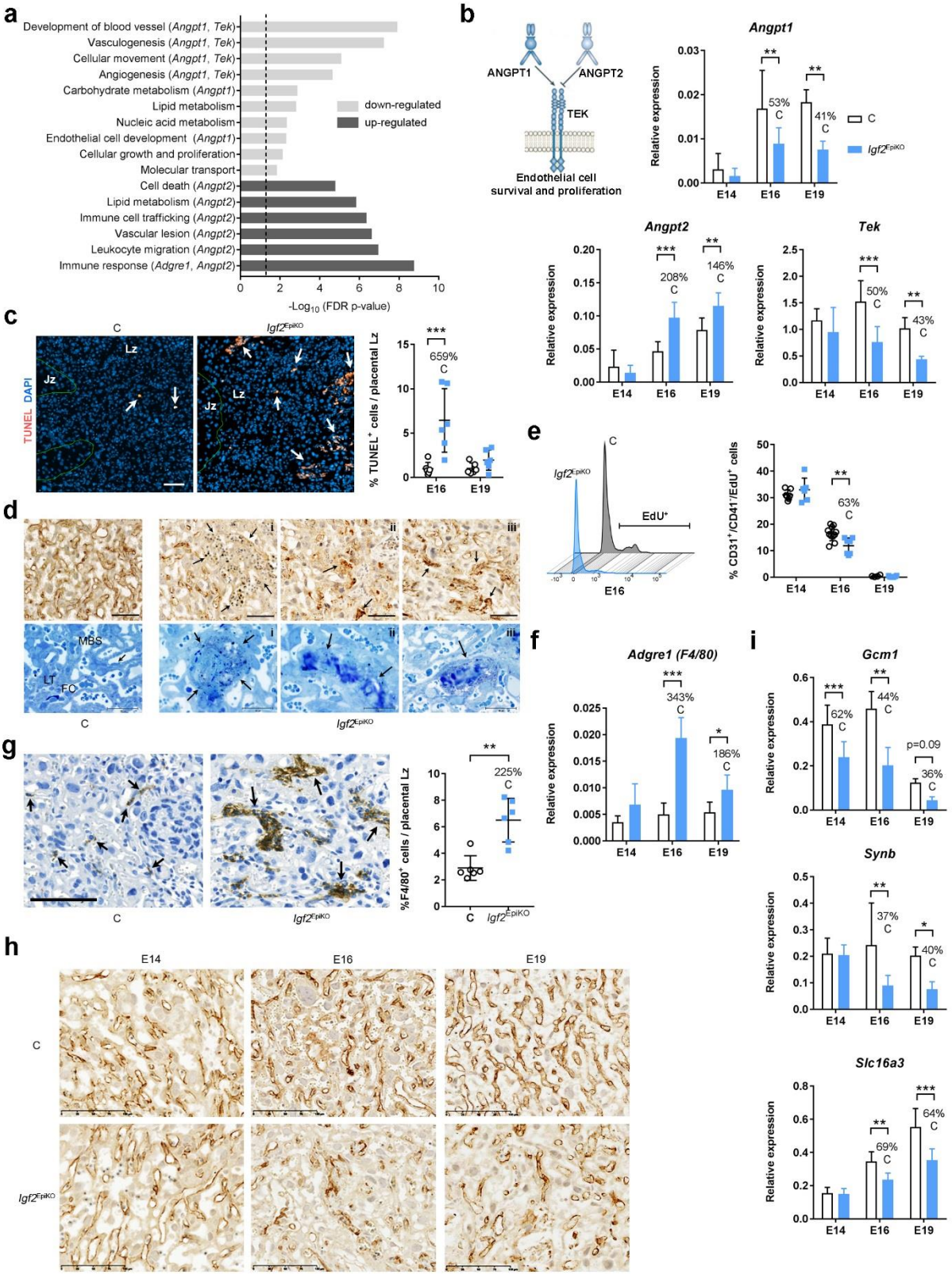


**Figure 3: Lack of fetus-derived IGF2 reduces the expansion of feto-placental microvasculature in late gestation.**

**a,** Functions enriched in DEGs at E19. **b,** qRT-PCR analysis of angiopoietin-Tie2/TEK signalling components in placental Lz (n=6–8 per group). **c,** TUNEL staining in E16 placental Lz (arrows point to apoptotic cells) and data quantification (n=6 samples per group); scale bar is 50µm. **d,** Top row: CD31 staining in control (C) and *Igf2*$^{EpiKO}$ mutant E16 placental Lz illustrating abnormally large FCs lacking endothelial cells (i) or obstructed capillaries surrounded by fragmented and disorganized FPEC (ii, iii). Scale bars are 50µm. Bottom row: methylene blue-stained E16 placental Lz resin sections (arrows indicate a FPEC in C and thrombotic FC in mutants: i-iii). Scale bars are 30µm. **e,** FPEC proliferation measured by flow cytometry (left – representative histograms at E16; right – data quantification; n=4–11 per group). **f,** qRT-PCR analysis of *Adgre1* in placental Lz. **g,** Representative F4/80 immunostainings in E16 placental Lz (arrows indicate macrophages). Scale bar is 100µm. Right: percentage of macrophages/placental Lz at E16 (n=6–8 samples per group). **h,** Representative CD31 immunostaining in placental Lz (scale bar is 100µm). **i,** Top: qRT-PCR analysis for SynT-II (syncytiotrophoblast layer II) marker genes. For all graphs data is presented as averages or individual values; error bars are SD; * $P$<0.05, ** $P$<0.01, *** $P$<0.001 by two-way ANOVA plus Sidak's multiple comparisons tests (**b**, **c**, **e**, **f**, **i**) or Mann-Whitney tests (**g**).

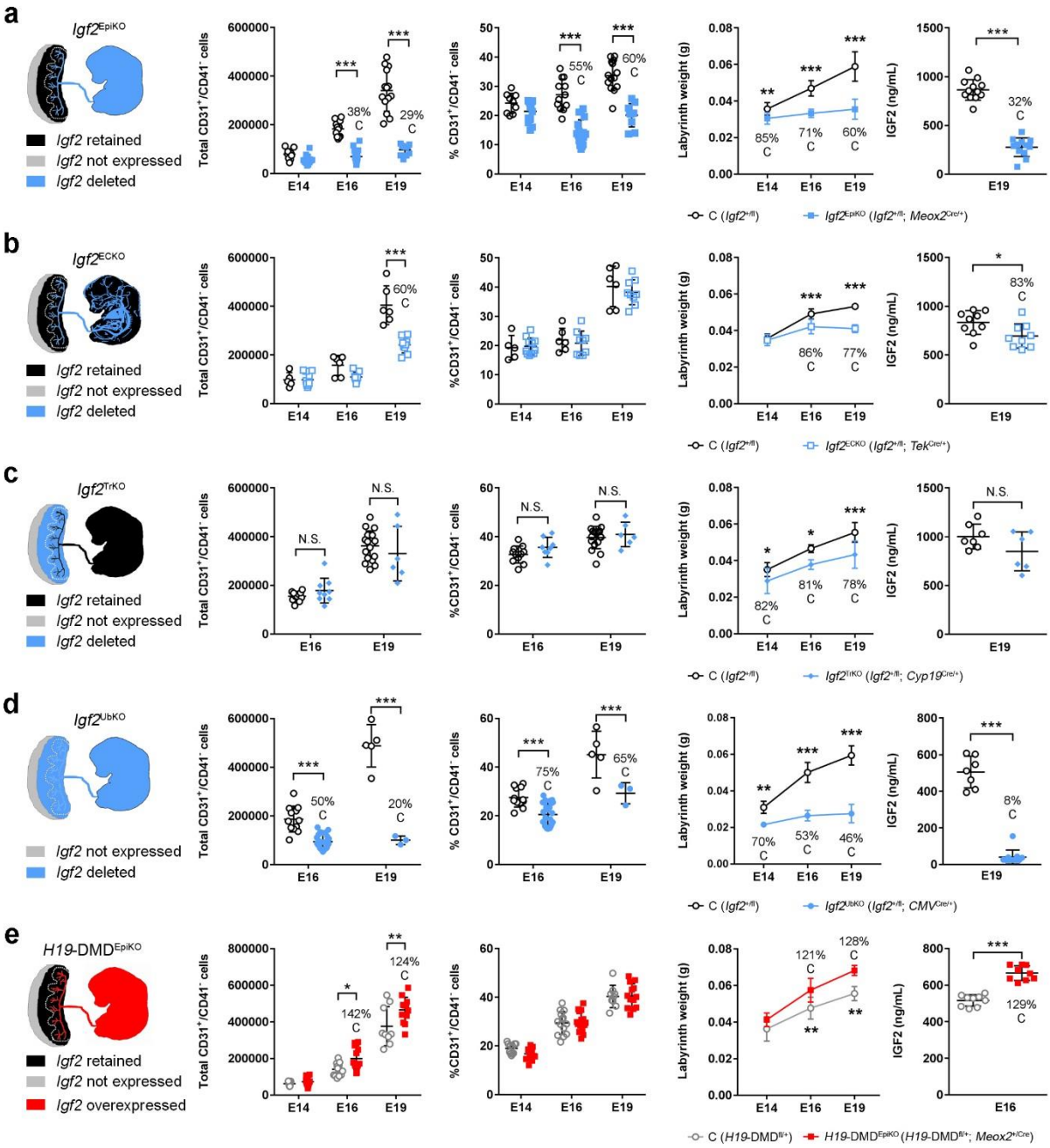


**Figure 4: Genetic models of mismatched supply and demand reveal circulating IGF2 as a major endocrine regulator of FPEC and placental Lz expansion.**

Column 1: schematic diagram of the genetic models: *Igf2*$^{EpiKO}$ (**a**), *Igf2*$^{ECKO}$ (**b**), *Igf2*$^{TrKO}$ (**c**), *Igf2*$^{UbKO}$ (**d**) *H19*-DMD$^{EpiKO}$ (**e**). Columns 2 and 3: total numbers (column 2) and proportion of FPEC/placental Lz (column 3), measured by flow cytometry (n conceptuses per group: *Igf2*$^{EpiKO}$: n=9–18; *Igf2*$^{ECKO}$: n=5–11; *Igf2*$^{TrKO}$: n=6–17; *Igf2*$^{UbKO}$: n=3–26; *H19*-DMD$^{EpiKO}$: n=9–15). Column 4: placental Lz growth kinetics (*Igf2*$^{EpiKO}$: n=9–20 litters; *Igf2*$^{ECKO}$: n=3–9 litters; *Igf2*$^{TrKO}$: n=4–9 litters; *Igf2*$^{UbKO}$: n=3–8 litters; *H19*-DMD$^{EpiKO}$: n=3–4 litters). Column 5: IGF2 levels (ng/mL) in plasma (n per group: *Igf2*$^{EpiKO}$: n=12; *Igf2*$^{ECKO}$: n=9; *Igf2*$^{TrKO}$: n=6–7; *Igf2*$^{UbKO}$: n=7–11; *H19*-DMD$^{EpiKO}$: n=9). Data is shown as averages or individual values and error bars are SD. N.S. – not significant; * $P$<0.05; ** $P$<0.01; *** $P$<0.001 calculated by two-way ANOVA plus Sidak's multiple comparisons tests (second, third and fourth columns) or Mann Whitney tests (fifth column).

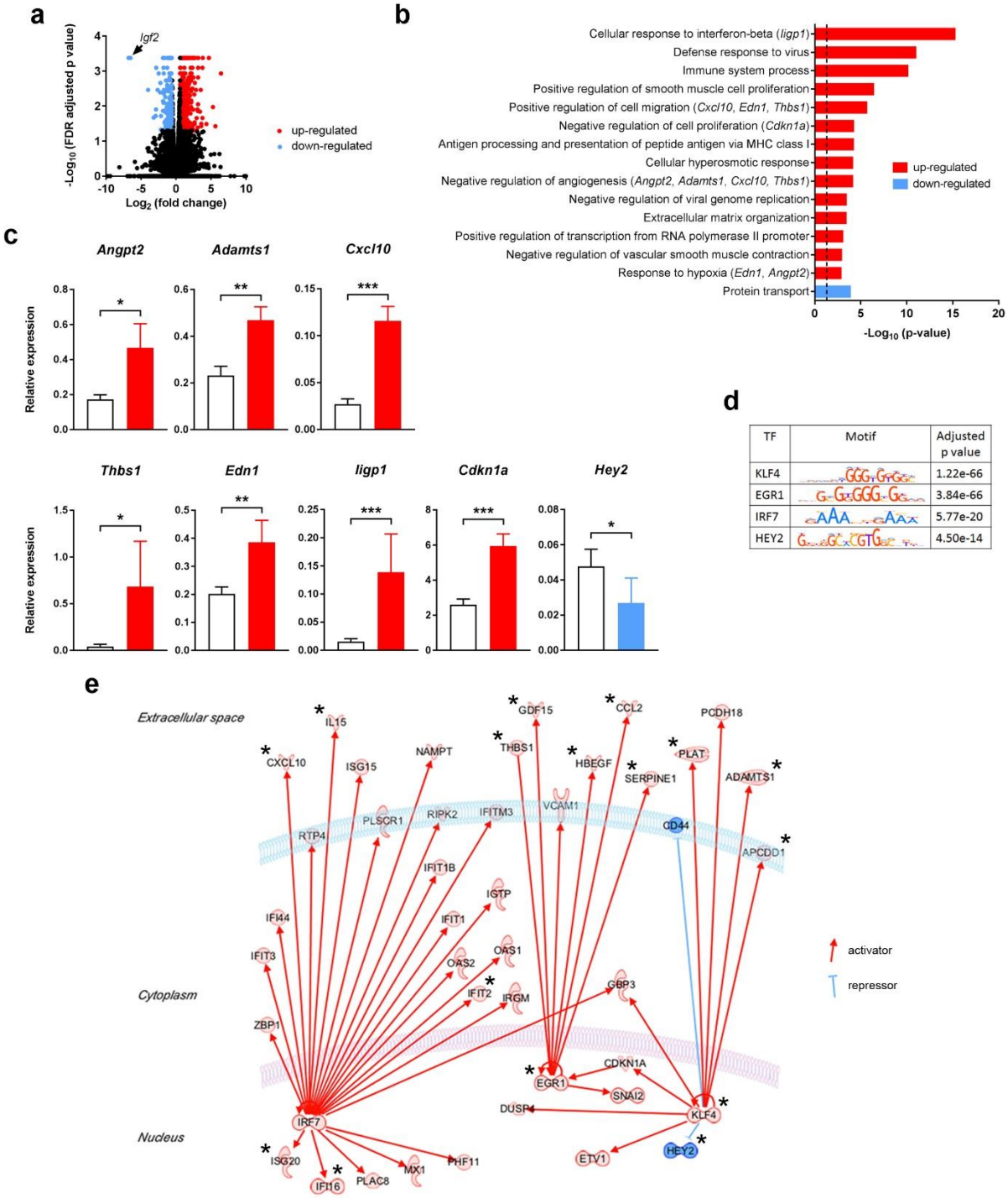


729

730

731 **Figure 5: IGF2 signalling regulates angiogenic properties of endothelial cells.**

732 **a,** Volcano plot representation of DEGs identified by RNA-seq in E16 FPEC (*Igf2*$^{EpiKO}$ versus controls).
733 Significant up-regulated (red) and down-regulated (blue) DEGs (FDR<0.05). **b,** Top scoring biological
734 processes enriched in DEGs. Biologically validated DEGS are listed in parentheses. The dotted line
735 corresponds to FDR-corrected *P* value of 0.05. **c**, Biological validation. Data is shown as averages (n=11-
736 12 samples per group); error bars are SEM; * *P*<0.05, ** *P*<0.01, *** *P*<0.001 calculated by Mann-
737 Whitney tests. **d,** Transcription factors (TFs) identified by Analysis of Motif Enrichment (AME) **e**, IPA
738 regulatory network built with the four TFs identified using AME analysis. Proteins labelled with * are

known regulators of angiogenesis (angiostatic or pro-angiogenic factors) and key references are listed in Supplementary Table 4.

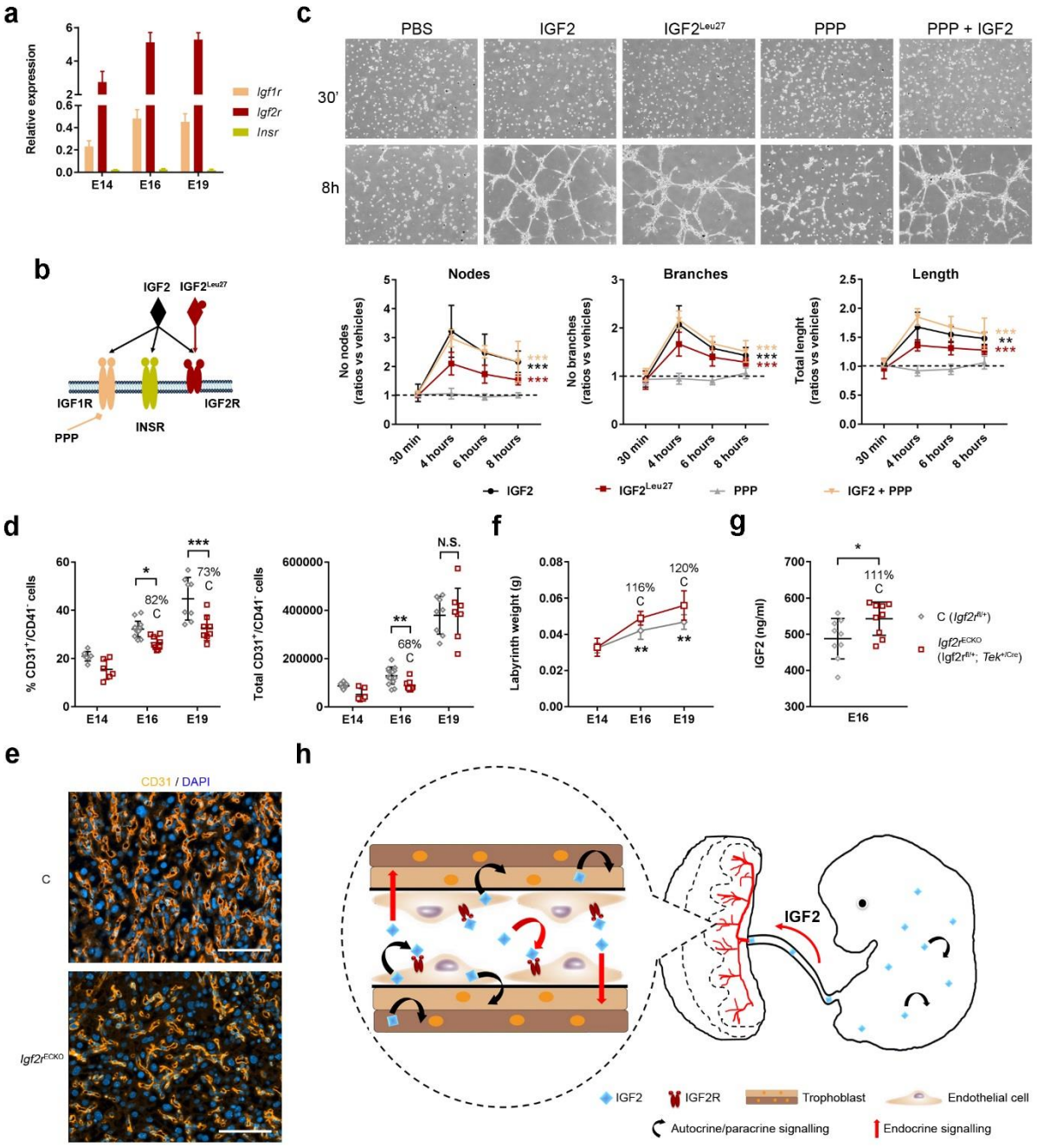


**Figure 6: IGF2 acts on feto-placental endothelial cells via IGF2R both *in vitro* and *in vivo*.**

**a,** qRT-PCR analysis for *Igf1r*, *Igf2r* and *Insr* in primary FPEC (n=6–7 per group). **b,** Schematic representation of IGF2 and IGF receptors. IGF2$^{Leu27}$ analogue acts specifically on IGF2R and picropodophyllin (PPP) inhibits phosphorylation of IGF1R. **c,** Representative images of capillary-like tube formation assay in primary FPEC seeded on matrigel and exposed to exogenous IGF2, IGF2$^{Leu27}$,

PPP or PPP+IGF2 (equal seeding of cell numbers at 30' and tube formation at 8h), and quantification of number of nodes, branches and total length (n=5–6 independent experiments). **d,** Proportion and total numbers of FPEC/placental Lz measured by flow cytometry (n=6–14 per group). **e,** Representative CD31 immunofluorescence staining in E16 placental Lz (scale bar is 100µm). **f,** Placental Lz growth kinetics: *Igf2r*$^{ECKO}$ (n=8–16 conceptuses per group). **g,** IGF2 levels (ng/mL) in plasma at E16 (n=9 per group). **h,** Model summarizing the proposed actions of fetus-, endothelial- and trophoblast-derived IGF2. For all graphs, data is presented as averages or individual values and error bars represent SD (**a**, **d**, **e**, **g**) or SEM (**c**). N.S. – not significant; * $P$<0.05; ** $P$<0.01; *** $P$<0.001 calculated by two-way ANOVA tests (**c**); two-way ANOVA plus Sidak's multiple comparisons tests (**d**, **f**) or Mann Whitney tests (**g**).

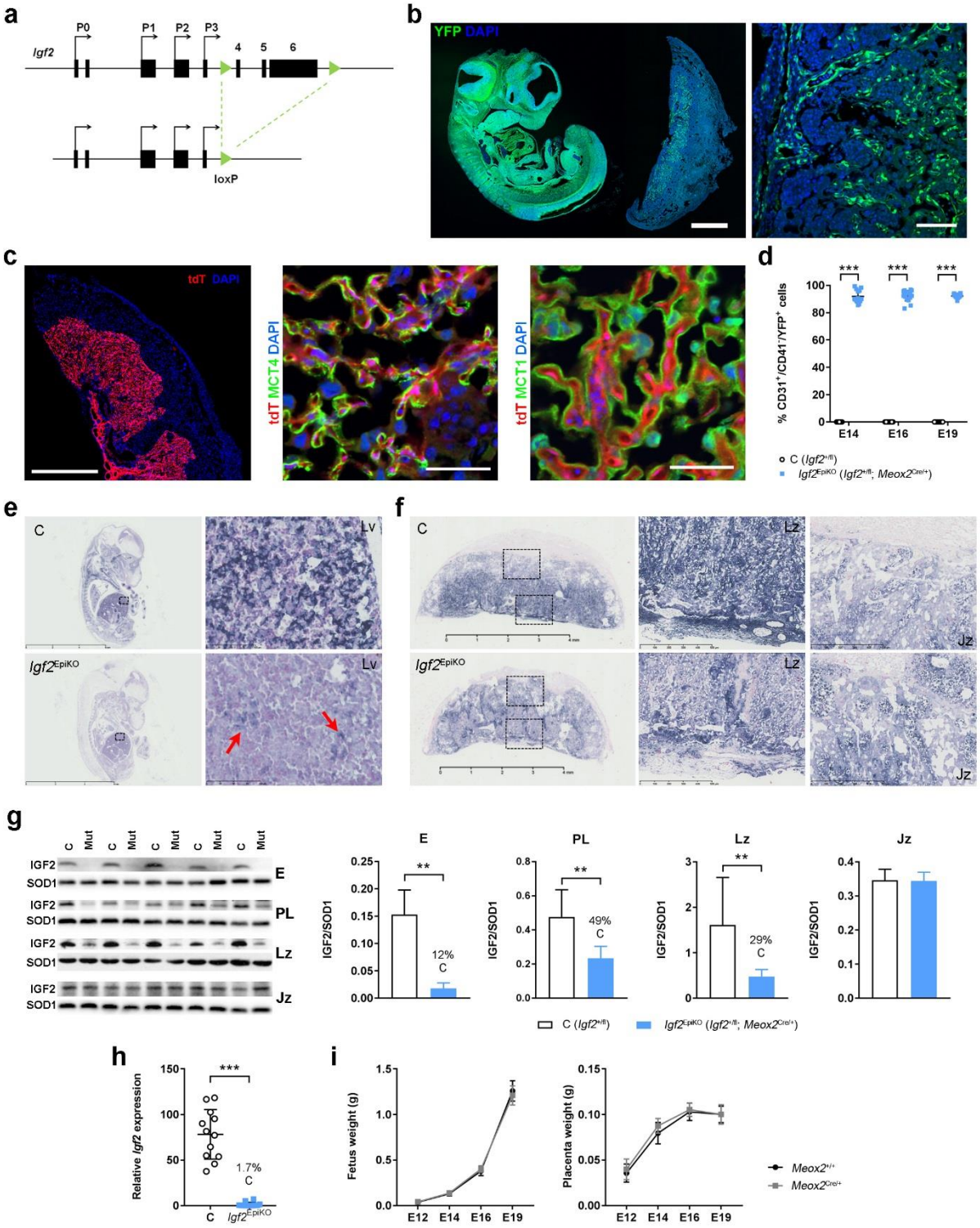


**Extended Data Figure 1: Specificity and efficiency of *Igf2* deletion in fetal tissues and feto-placental endothelial cells by *Meox2*$^{Cre}$.**

**a,** Schematic representation of the floxed *Igf2* allele. P0-P3 are alternative promoters. Protein-coding exons (4–5), flanked by loxP sites (green triangles), are excised upon Cre-loxP mediated recombination. **b,** Immunostaining for YFP (green) in a representative fetus and placenta at E12 of gestation, double transgenic for *Meox2*$^{Cre}$ and *Rosa26* $^{fl}$STOP$^{fl}$YFP[10] reporter. YFP expression is observed throughout the fetus and in the placenta is localized to the labyrinthine zone and chorionic

plate (right panel). Blue – DAPI stain for nuclei; scale bars are 1 mm (left) and 100 µm (right). **c,** Representative confocal microscopy of a placental frozen section at E16 of gestation, double transgenic for *Meox2*$^{Cre}$ and Ai9(RCL-tdT) reporter. The *Meox2*$^{Cre}$ is not expressed in the syncytiotrophoblast layers, as demonstrated by the lack of immunostaining overlap between the tomato protein (red) and MCT4 (a marker of the syncytiotrophoblast layer II, facing the feto-placental capillaries) or MCT1 (marker of the syncytiotrophoblast layer I, facing the maternal blood spaces). Scale bars are 1 mm (left panel) and 50 µm (middle and right panels). **d,** Flow cytometry analysis shows that the majority (>80%) of *Igf2*$^{EpiKO}$ mutant FPEC (CD31$^{+}$/CD41$^{-}$ cells) express YFP (activated by *Meox2*$^{Cre}$ mediated deletion of the *Rosa26* $^{fl}$STOP$^{fl}$YFP STOP cassette), thus demonstrating good efficiency of *Meox2*-Cre in these cells (n=9–18 per genotype). **e,** *Igf2* mRNA in situ hybridization (ISH) in E14 control and mutant fetuses. Dark blue indicates *Igf2* mRNA, with nuclei marked in red. Insets illustrate efficient *Igf2* deletion in the liver (Lv); arrows – small pockets of cells with incomplete *Igf2* deletion (mosaic activity of *Meox2*$^{Cre}$). Scale bars are 6 mm (left) and 100 µm (right). **f,** *Igf2* mRNA ISH in E14 control and mutant placentae. Insets show reduced *Igf2* mRNA signal in the placental labyrinthine zone (Lz) of mutants, due to its deletion from FPEC, while *Igf2* expression is unchanged in the junctional zone (Jz). Scale bars are 4 mm (left) and 500 µm (right). **g,** Western blot analysis of pro-IGF2 (18kDa) in cell lysates from whole fetuses (F), whole placenta (PL) micro-dissected placental labyrinthine (Lz) and junctional zones (Jz) at E14, and corresponding data quantification shown as graphs (n=5 per genotype). SOD1 (19 kDa) was used as loading control. **h,** Efficiency of *Igf2* deletion evaluated by qRT-PCR in fluorescence-activated sorted FPEC (n=12 per genotype). **i,** Fetal and placental growth kinetics are not altered in *Meox2*$^{Cre/+}$ carriers (maternal inheritance) (n=8–30 conceptuses per genotype at each developmental stage). For all graphs, data is shown as individual values or averages ± SD; ** $P < 0.01$, *** $P < 0.001$ calculated by two-way ANOVA plus Sidak's multiple comparisons tests (**d**) or Mann Whitney tests (**g**, **h**).

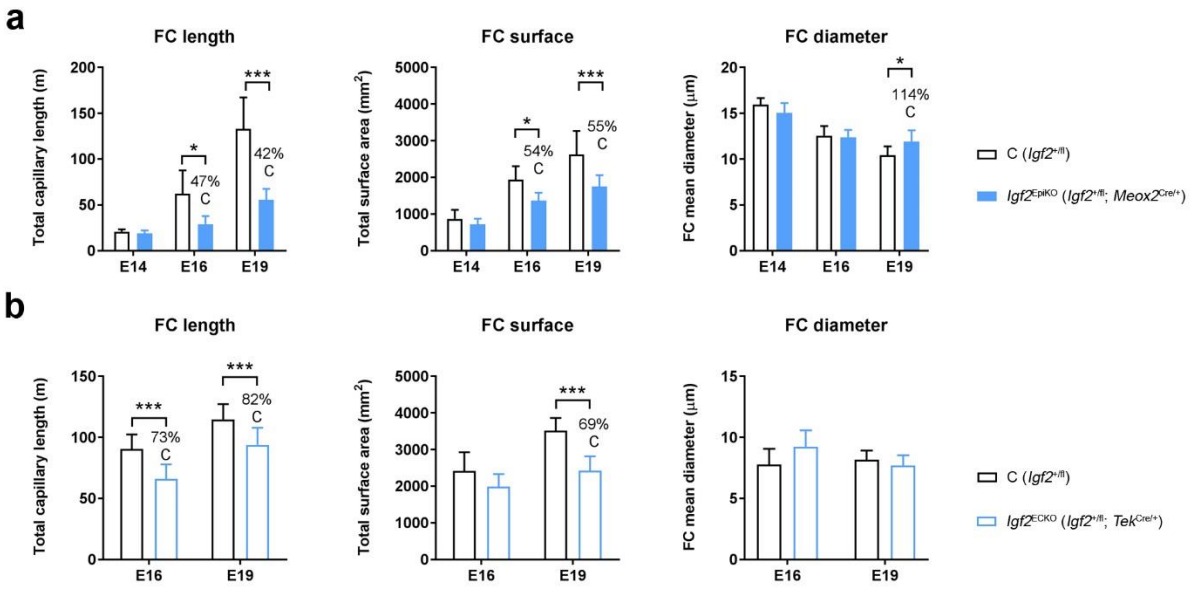


**Extended Data Figure 2: Impact of *Igf2*$^{EpiKO}$ and *Igf2*$^{ECKO}$ deletions on feto-placental capillary expansion during gestation.**

**a,** Parameters of feto-placental capillaries (FC) measured by stereology in *Igf2*$^{EpiKO}$ mutant (*Igf2*$^{+/fl}$; *Meox2*$^{Cre/+}$) versus control (C – *Igf2* $^{+/fl}$) placentae (n=6 per genotype at each developmental stage). **b,** Parameters of feto-placental capillaries (FC) measured by stereology in *Igf2*$^{ECKO}$ mutant (*Igf2*$^{+/fl}$; *Tek*$^{Cre/+}$) versus control (C – *Igf2* $^{+/fl}$) placentae (n=5–7 per genotype at each developmental stage). For all graphs, data is shown as averages ± SD; * $P < 0.05$, *** $P < 0.001$ calculated by two-way ANOVA plus Sidak's multiple comparisons tests.

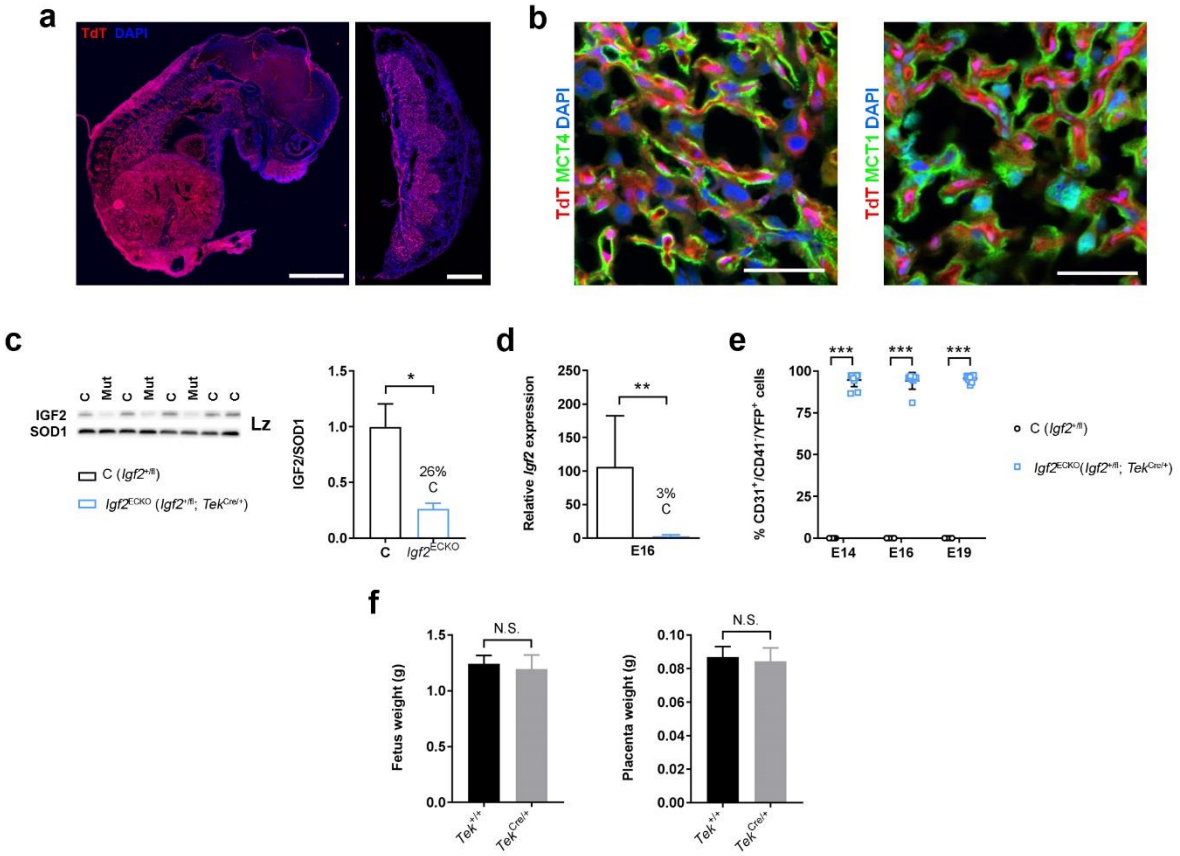


**Extended Data Figure 3: Specificity and efficiency of *Igf2* deletion in the endothelium by *Tek*$^{Cre}$.**

**a,** Representative confocal microscopy of frozen sections from a fetus and corresponding placenta, double transgenic for *Tek*$^{Cre}$ and Ai9(RCL-tdT) reporter at E16 of gestation. Scale bars are 2 mm (fetus) and 1 mm (placenta). **b,** The *Tek*$^{Cre}$ is not expressed in the syncytiotrophoblast layers, as demonstrated by the lack of immunostaining overlap between the tomato protein (red) and MCT4 (Syn-TII layer) or MCT1 (Syn-TI layer). Scale bars are 50 µm. **c,** Western blot analysis of pro-IGF2 (18 kDa) in cell lysates from placental Lz micro-dissected at E16 and corresponding data quantification (n=3 per genotype). SOD1 (19 kDa) was used as internal control for loading. **d,** Efficiency of *Igf2* deletion evaluated by qRT-PCR in fluorescence-activated sorted FPEC (n=5–7 per genotype). **e,** Flow cytometry analysis shows that the majority (>80%) of *Igf2*$^{ECKO}$ mutant FPEC express YFP, thus demonstrating good efficiency of *Tek*$^{Cre}$ in these cells (n=5–11 per genotype). **f,** Fetal and placental growth kinetics are not altered in *Tek*$^{Cre/+}$ carriers (maternal inheritance) at E19 (n=13–15 conceptuses per genotype from 4 independent litters).

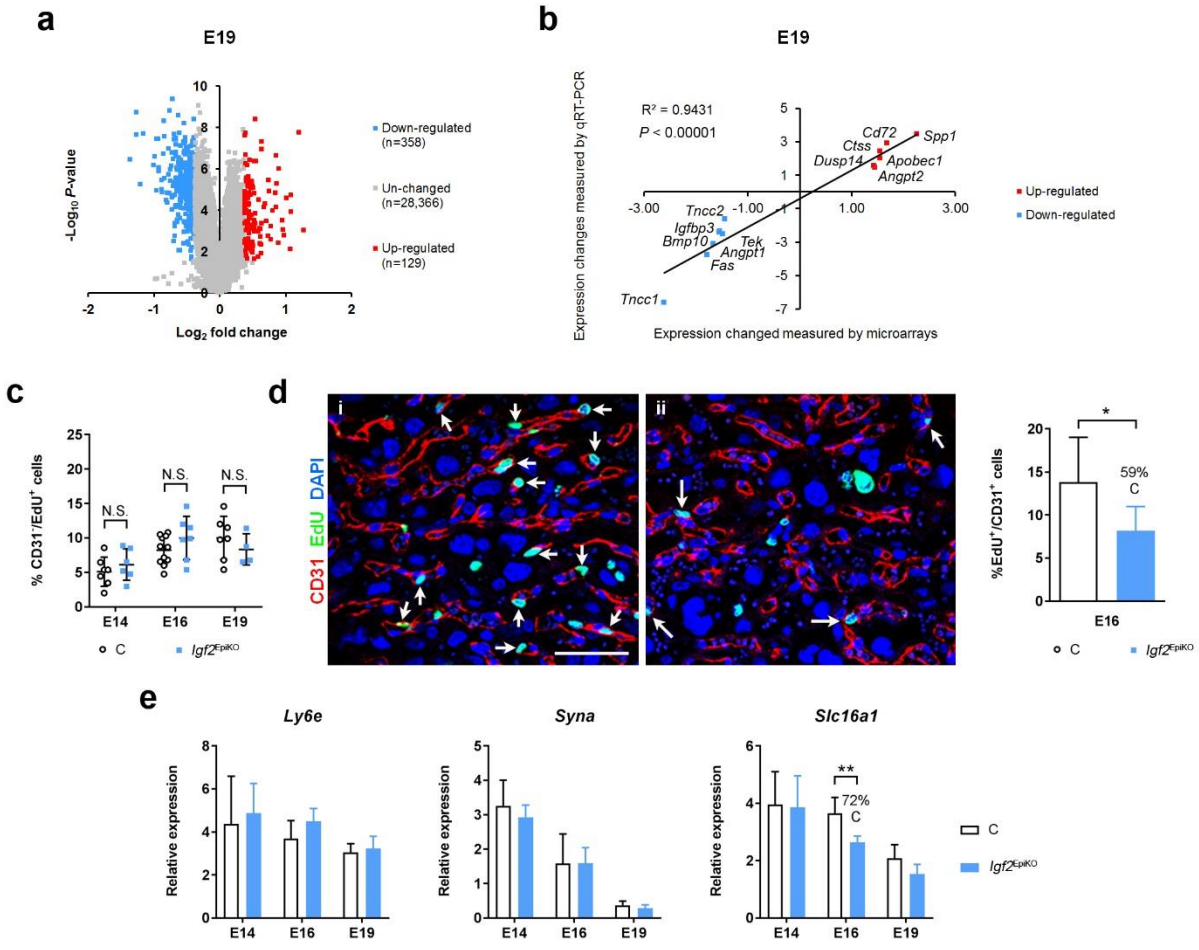


**Extended Data Figure 4: Fetus-derived *Igf2* deletion (*Igf2*$^{EpiKO}$) alters gene expression in placental Lz and FPEC proliferation.**

**a,** Volcano plot depicting differentially expressed genes (DEG) identified in E19 placental Lz by expression microarray analysis (n=6 samples per genotype, all from male conceptuses). **b,** Biological validation using qRT-PCR for 13 DEGs (n=6–7 samples per genotype), normalized against three housekeeping genes (*Sdha*, *Gapdh* and *Pmm1*). **c,** The reduction in proliferation seen in FEPC (Fig. 3e) is not observed in non-endothelial cells from placental Lz measured by flow cytometry analysis after EdU injections (16 hours exposure; n=4–11 per group). **d,** Representative confocal microscopy image of FPEC proliferation in control (panel i) versus mutant (panel ii) E16 placentae by immunofluorescent staining for CD31 combined with Click-iT EdU imaging. Arrows point towards FPEC nuclei that incorporated EdU *in vivo* during the 16 hours exposure to the thymidine analogue. Scale bar is 50 µm. The accompanying graph shows data quantification based on counting between 250 to 600 FPEC per sample (n=6 placentae/genotype). **e,** qRT-PCR analysis of genes expressed in Syn-TI in micro-dissected placental Lz in mutants versus controls (n=6–8 samples per group for each developmental time point). For all graphs, data is presented as averages or individual values ± SD; N.S. – non-significant, * $P < 0.05$, ** $P < 0.01$, by two-way ANOVA plus Sidak's multiple comparisons tests (**c**, **e**) or Mann Whitney test (**d**).

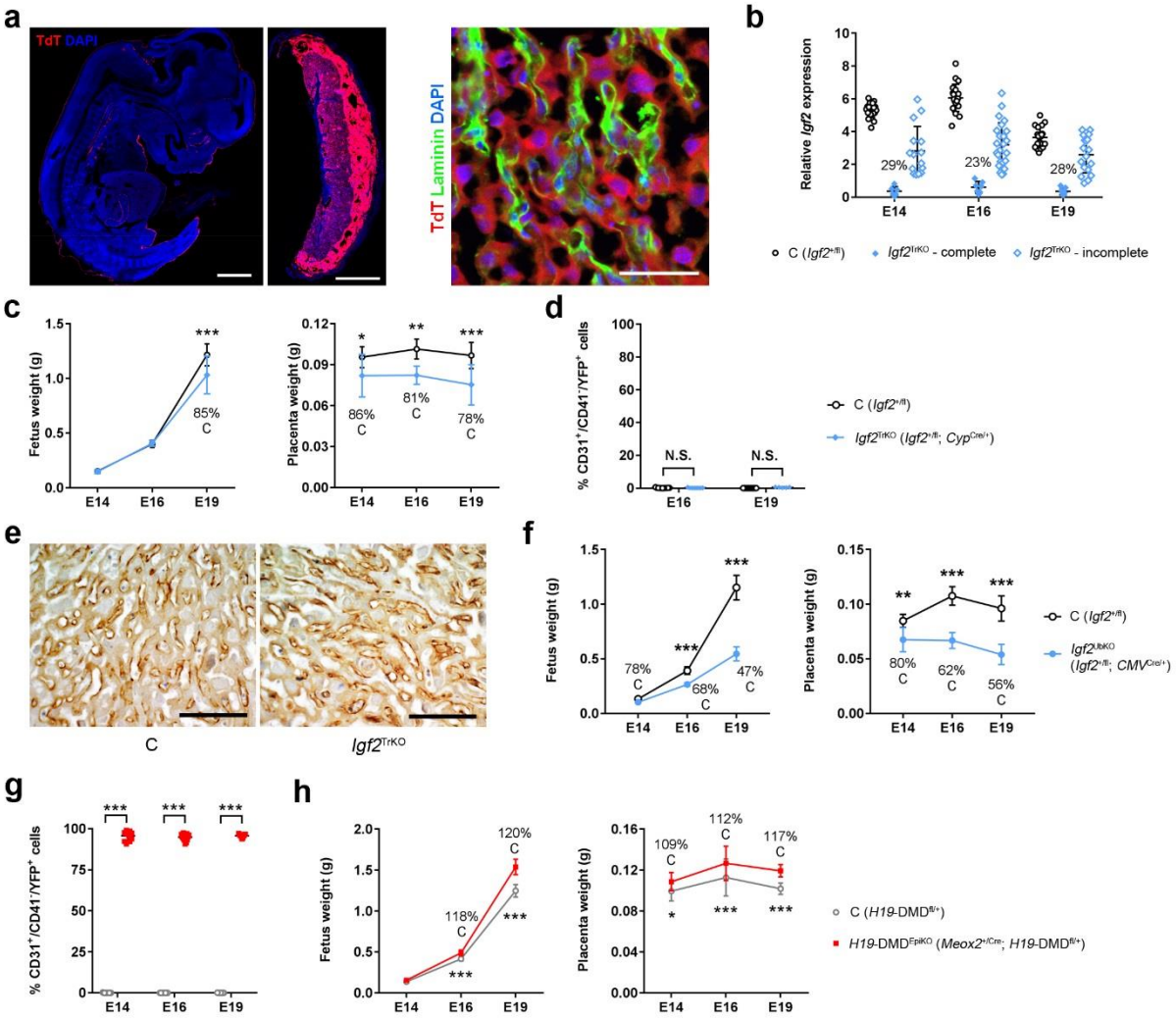


**Extended Data Figure 5: Specificity and efficiency of *Igf2*$^{TrKO}$, *Igf2*$^{UbKO}$ and *H19*-DMD$^{EpiKO}$ deletions.**

**a,** Representative confocal microscopy on frozen sections from a double transgenic Ai9(RCL-tdT), *Cyp19*$^{Cre}$ fetus and corresponding placenta, at E16, demonstrating high Cre activity (red) in placenta and weak activity in embryonic skin and eye lenses. Right panel: *Cyp19*$^{Cre}$ is only active in the trophoblast cells in placental Lz, as demonstrated by lack of overlapping between the tomato protein (red) and laminin (green) expressed in FPEC. Scale bars are 1 mm (left and middle panel) or 50 µm (right panel). **b,** Efficiency of *Igf2* deletion by *Cyp19*$^{Cre}$ in *Igf2*$^{TrKO}$ mutants (*Igf2*$^{+/fl}$; *Cyp19*$^{Cre/+}$) versus controls (*Igf2*$^{+/fl}$) evaluated using qRT-PCR in micro-dissected placental Jz layer (n=20–31 samples per genotype). Only 23-29% of all *Igf2*$^{TrKO}$ mutants have high levels of deletion (>80%). **c,** Placenta growth restriction precedes fetal growth restriction in *Igf2*$^{TrKO}$ mutants (n=4–9 litters at each developmental stage; only mutants with >80% deletion were included in this analysis). **d,** Flow cytometry analysis showing that *Cyp19*$^{Cre}$ is not expressed in FPEC (note lack of YFP expression in *Igf2*$^{TrKO}$ mutants) (n=6–21 per genotype). **e,** Representative CD31 immunostainings in E16 control and *Igf2*$^{TrKO}$ placental Lz (scale bars are 100µm) showing no impact of the deletion on FPEC numbers. **f,** Severe fetal and placental growth restriction in *Igf2*$^{UbKO}$ (*Igf2*$^{+/fl}$; *CMV*$^{Cre/+}$) mutants (n=3-8 litters at each developmental stage). **g,** Flow cytometry analysis shows that the majority (>80%) of *H19*-DMD$^{EpiKO}$ (*Meox2*$^{+/Cre}$; *H19*-DMD$^{fl/+}$) mutant FPEC express YFP, demonstrating good efficiency of *Meox2*$^{Cre}$ in these cells (n=9–15 per genotype). **h,** Fetal and placental overgrowth in *H19*-DMD$^{EpiKO}$ mutants (n=3-4 litters at each

developmental stage). For all graphs, data is shown as averages or individual values ± SD. N.S. – non-significant, * $P < 0.05$; ** $P < 0.01$; *** $P < 0.001$ calculated by two-way ANOVA plus Sidak's multiple comparisons tests (**b**, **c**, **d**, **f**, **g**, **h**).

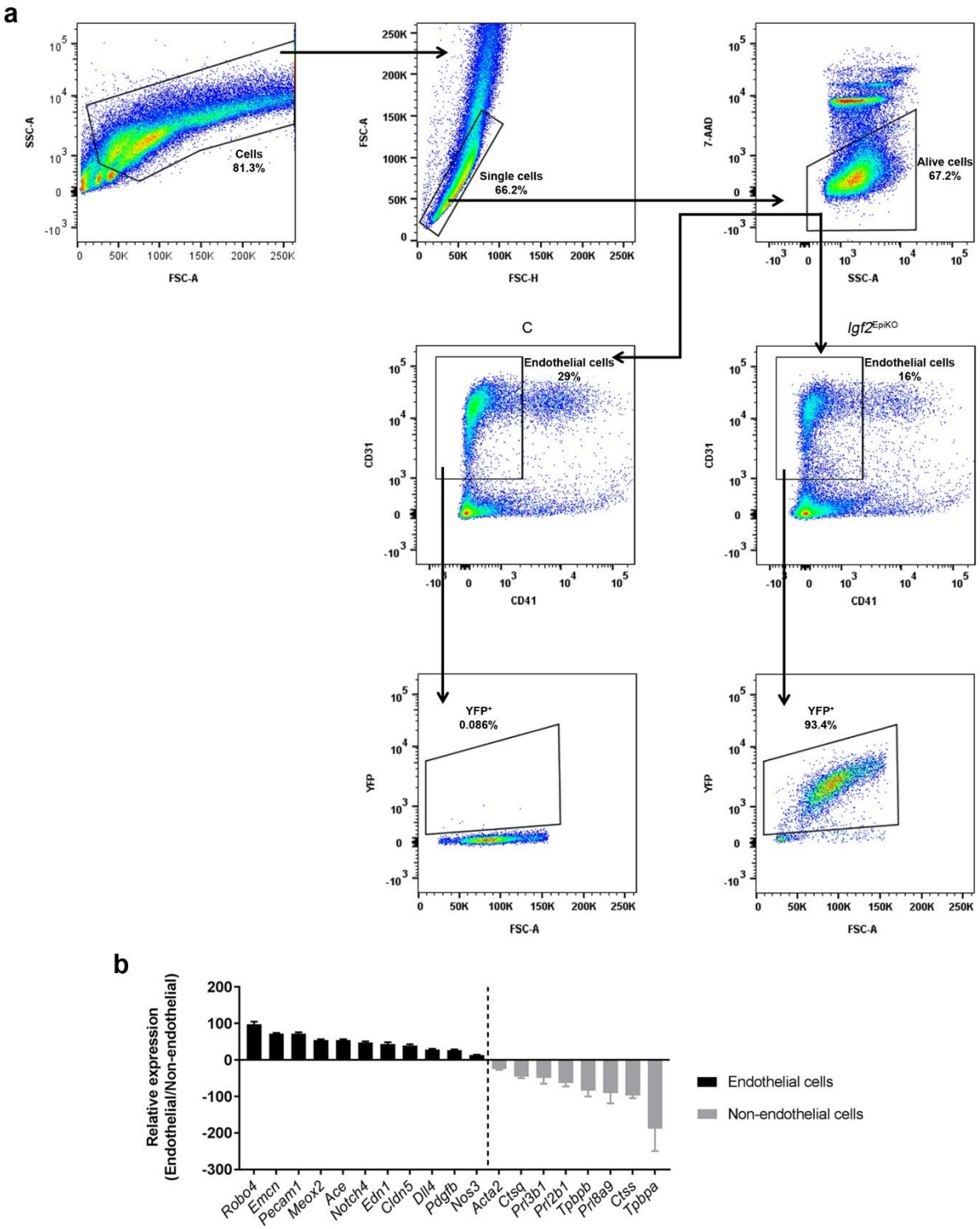


**Extended Data Figure 6: Experimental design used for FPEC analysis by flow cytometry and FPEC isolation by FACS.**

**a,** Gating strategy used for flow cytometry analysis of FPEC and their isolation by FACS. FPEC are defined as viable, single cells positive for CD31 and negative for CD41. Mutant FPEC are also positive for YFP (activated by Cre mediated deletion of the *Rosa26* $^{fl}$STOP$^{fl}$YFP STOP cassette), thus providing an internal control for Cre efficiency in each biological sample. **b,** RNA-seq analysis of marker genes expressed in FPEC or non-endothelial cells isolated by FACS from E16 control placental Lz. The graph shows the relative enrichment in FPEC of known markers of endothelial cells (black) and depletion of marker genes expressed by other cell types found in the placental Lz (grey): pericytes (*Acta2*), sinusoidal trophoblast giant cells (*Ctsq*, *Prl2b1*, *Prl8a9*), parietal trophoblast giant cells (*Prl3b1*) or spongiotrophoblast cells (*Tpbpa*, *Tpbpb*).

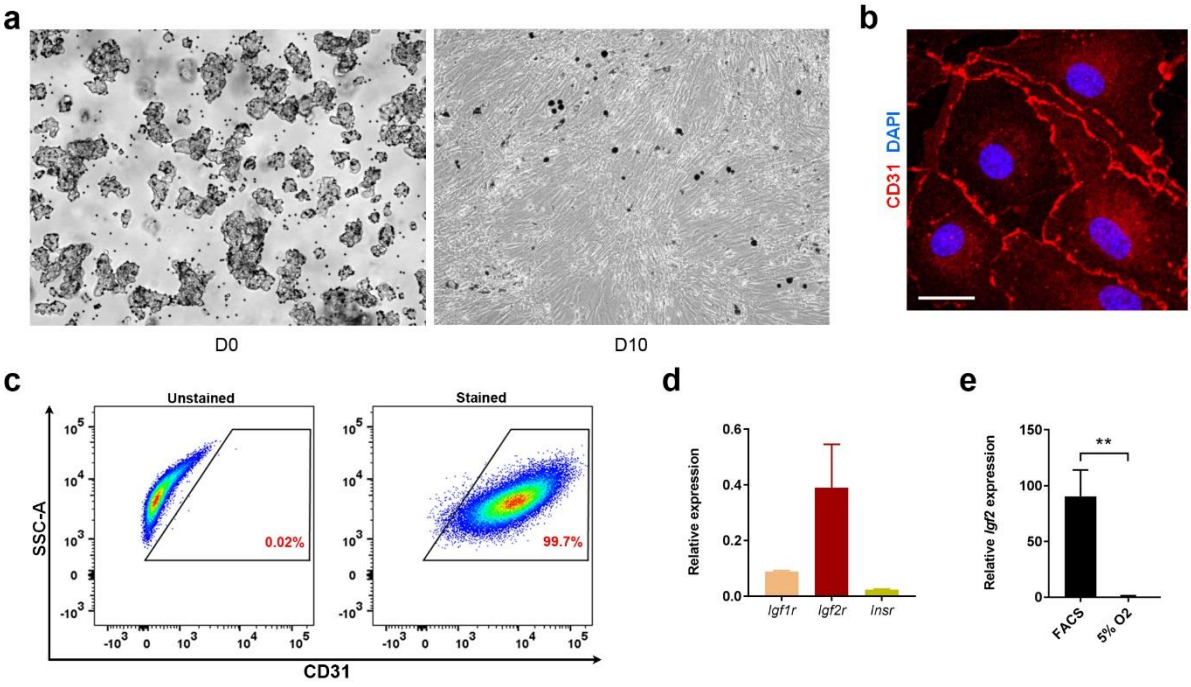


**Extended Data Figure 7: *Ex vivo* culture of primary FPEC isolated from E16 placental Lz.**

**a,** Primary FPEC isolated from E16 placental Lz: D0 – freshly isolated cells, bound to magnetic beads coated with anti-CD31 antibodies; D10 – FPEC at passage one (after approximately 10 days of culture). **b,** Confocal imaging of passage one FPEC, stained for CD31 (scale bar is 20 µm). **c,** Flow cytometry analysis of passage one FPEC stained for CD31, demonstrating that these are almost exclusively CD31$^{+}$. **d,** Relative expression of the three IGF receptors in passage one FPEC. **e,** qRT-PCR analysis of *Igf2* mRNA levels in passage one FPEC cultured in 5% O2 versus primary FPEC isolated from E16 placental Lz by FACS. For panels **d** and **e** data is presented as average values ± SEM (n=6 samples per group); ** $P < 0.01$ using a Mann Whitney test (**e**).

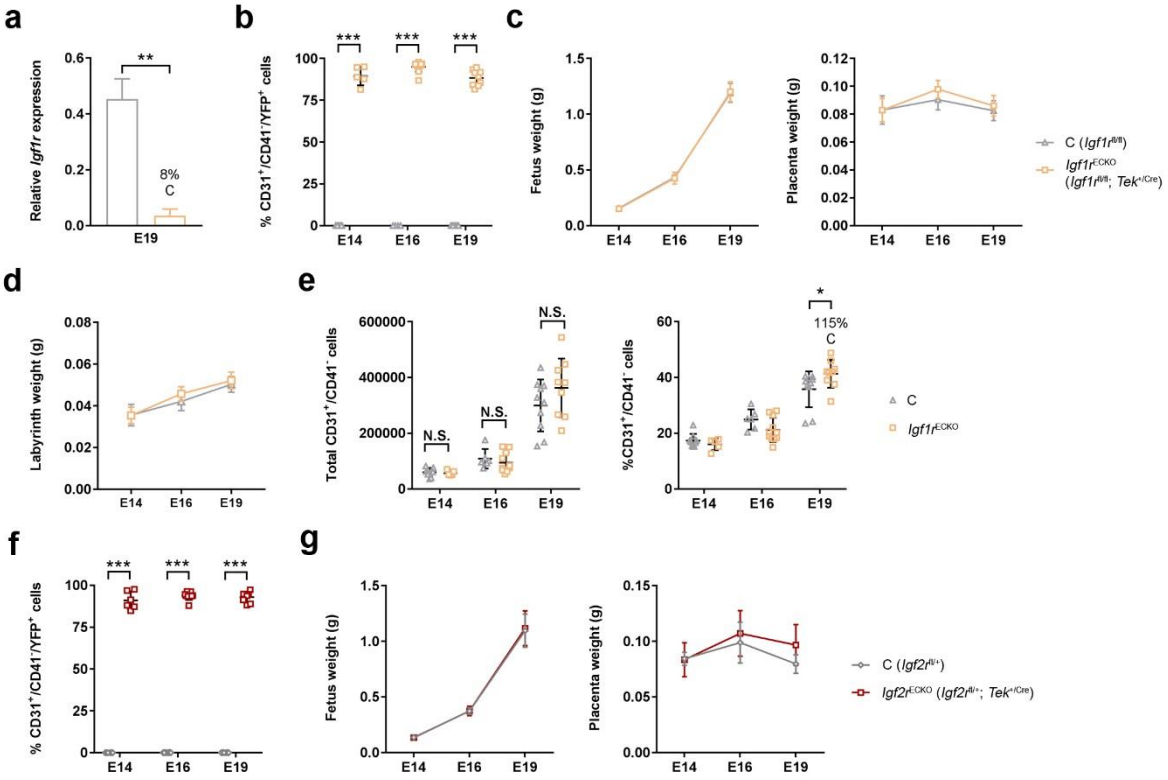


**Extended Data Figure 8: Conditional deletions of *Igf1r and Igf2r* from endothelium using *Tek*$^{Cre}$.**

**a,** qRT-PCR analysis of *Igf1r* mRNA levels in primary FPEC isolated by FACS from E19 placental Lz of *Igf1r*$^{ECKO}$ (*Igf1r*$^{fl/fl}$; *Tek*$^{+/Cre}$) mutants versus *Igf1r*$^{fl/fl}$ controls. **b,** Flow cytometry analysis showing that the majority (>80%) of *Igf1r*$^{ECKO}$ mutant FPEC express YFP, demonstrating good efficiency of *Tek2*$^{Cre}$ in these samples (n=5–11 per genotype). Fetal, placental (**c**) and placental Lz (**d**) growth kinetics are not altered in *Igf1r*$^{ECKO}$ mutants compared to controls (n=6–18 conceptuses from n=3-7 litters for each developmental stage). **e,** Total numbers and proportions of FPEC/placental Lz measured by flow cytometry (n=5–11 per genotype). **f,** Flow cytometry analysis showing that the majority (>80%) of *Igf2r*$^{ECKO}$ mutant FPEC express YFP, demonstrating good efficiency of *Tek2*$^{Cre}$ in these samples (n=6–14 per genotype). **g,** Fetal and placental growth kinetics are unaltered in *Igf2r*$^{ECKO}$ (*Igf2r*$^{fl/+}$; *Tek*$^{+/Cre}$) mutants compared to *Igf2r*$^{fl/+}$ controls (n=8–28 conceptuses from n=3-8 litters for each developmental stage). For all graphs, data is shown as individual values or averages ± SD; N.S. – non-significant, * $P < 0.05$, ** $P < 0.01$, *** $P < 0.001$ by Mann-Whitney tests (**a**) or two-way ANOVA plus Sidak's multiple comparisons tests (**b** – **g**).

**Supplementary Table 1**: Top 100 highest expressed genes by RNA-Seq from FACS purified E16 feto-placental endothelial cells. FPKM values represent the average of n=4 independent biological replicates. Paternally expressed and maternally expressed imprinted gene symbols are coloured in blue and red, respectively.

**Supplementary Table 2**: List of differentially expressed genes identified through expression microarray analysis in placental Lz samples micro-dissected from E19 *Igf2*$^{EpiKO}$ mutants (average of n=6) and controls (average of n=6). Upregulated and dowregulated gene symbols are coloured in blue and red, respectively.

**Supplementary Table 3**: List of differentially expressed genes by RNA-Seq from FACS purified feto-placental endothelial cells of E16 *Igf2*$^{EpiKO}$ mutants (average of n=4) and controls (average of n=4). Upregulated and downregulated gene symbols are coloured in blue and red, respectively.

**Supplementary Table 4: Angiostatic and pro-angiogenic factors produced by feto-placental endothelial cells under the control of fetus-derived IGF2**

| Protein | Expression change | Function (cellular compartment) | Role in angiogenesis | PMID |
|---|---|---|---|---|
| CXCL10 | Up-regulated | Cytokine (extracellular space) | angiostatic | 7537965, 7540647, 8611715, 9064358, 10914483 |
| IL15 | Up-regulated | Cytokine (extracellular space) | angiostatic | 28379958 |
| THBS1 | Up-regulated | | angiostatic | 22553494 |
| ADAMTS1 | Up-regulated | Peptidase (extracellular space) | angiostatic | 12716911, 12814950, 17082774, 22776012 |
| APCDD1 | Up-regulated | Membrane-bound glycoprotein (cellular membrane) | angiostatic | 29154126 |
| IFIT2 | Up-regulated | Interferon-induced protein (cytoplasm) | angiostatic | 26515391 |
| IFI16 | Up-regulated | Transcription regulator (nucleus) | angiostatic | 14729471, 21488755 |
| CCL2 | Up-regulated | Cytokine (extracellular space) | pro-angiogenic/ angiostatic if prolonged expression | 15516694, 16888027, 23329645 |
| EGR1 | Up-regulated | Transcription regulator (nucleus) | pro-angiogenic/ angiostatic if prolonged expression | 10339488, 12872165, 16818645, 27041221 |
| KLF4 | Up-regulated | Transcription regulator (nucleus) | pro-angiogenic/ angiostatic if prolonged expression | 24599951, 27431648, 26823670 |
| GDF15 | Up-regulated | Growth factor (extracellular space) | pro-angiogenic | 21773947, 28831101 |
| HBEGF | Up-regulated | Growth factor (extracellular space) | pro-angiogenic | 15289334, 18925469 |
| SERPINE1 | Up-regulated | Protease inhibitor (extracellular space) | pro-angiogenic | 26180080 |
| PLAT | Up-regulated | Peptidase (extracellular space) | pro-angiogenic | 24601228 |
| ISG20 | Up-regulated | Exonuclease (nucleus) | pro-angiogenic | 29195126 |
| HEY2 | Down-regulated | Transcription regulator (nucleus) | pro-angiogenic | 15107403, 16219802, 22421041 |

924 **Supplementary Table 5: Primers used for genotyping by PCR**

| Strain | Primer | Sequence | Primer | Sequence | Amplicon (bp) |
|---|---|---|---|---|---|
| *Igf2*$^{fl/fl}$ | F | TTACAGTTCAAAGCCACCACG | RW<br>RD | GCCAAAGAGATGAGAAGCACC<br>GCCAAACACAGTAAAAAGAAA TGC | WT: 324<br>fl: 449<br>del: 384 |
| *Rosa26* $^{fl}$*STOP*$^{fl}$*YFP* | F | TGTTATCAGTAAGGGAGCT | R-WT<br>R-fl | CACACCAGGTTAGCCTTTA<br>AAGACCGCGAAGAGTTTGT | WT: 239<br>fl: 301 |
| *Meox2*-Cre | F | GGACCACCTTCTTTTGGCTTC | R-WT<br><br>R-Cre | AAGATGTGGAGAGTACGGGGT AG<br>CAGATCCTCCTCAGAAATCAGC | WT: 410<br><br>Cre: 311 |
| *Tek*-Cre | F | TGTAAACAAGAGCGAGTGGA | R-WT<br>R-Cre | AGAGAATGGCGAGAAGTCAC<br>TGAGTGAACGAACCTGGTCG | WT: 240<br>Cre: 610 |
| *Cyp19*-Cre | F | GACCTTGCTGAGATTAGATC | R | AGAGAGAAGCATGTTTAGCTG G | Cre: 545 |
| *CMV*-Cre | F | CGAGTGATGAGGTTCGCAAG | R | TGAGTGAACGAACCTGGTCG | Cre: 390 |
| *H19*-DMD$^{fl/fl}$ | F | CAGGCCTGTCCTCACCTGAAC | R | GCCAGCTTGCCTTGGCAACCCC TT | WT: 387<br>fl: 520 |
| *Igf2r*$^{fl/fl}$ | F | CCTTCCCTCCAGGCCGTTAC | R | GGTGAGGTCTCCATCTGAGTAC C | WT: 225<br>fl: 259 |
| *Igf1r*$^{fl/fl}$ | F | CTTCCCAGCTTGCTACTCTAG G | R | CAGGCTTGCAATGAGACATGG G | WT: 124<br>fl: 220 |

925

926

927 **Supplementary Table 6: Conditions used for placenta immunostaining**

| Staining | Antigen retrieval | Blocking | Primary antibody | Secondary antibody |
|---|---|---|---|---|
| IGF2 | Digestion with 1% pronase (Protease from Streptomyces griseus, Sigma – P6911) in 1xPBS for 10 min at 37°C | 15% Donkey serum (Sigma – D9663) in PBS | Goat anti-human IGF2 (1:50, R&D systems AF-292) overnight at 4°C | AF488 Donkey anti-goat (1:200, Jackson ImmunoResearch – 705-546-147), one hour at room temperature |
| YFP | Autoclaving for 15 min at 121°C in citric acid buffer (10 mM citric acid, pH 6.0, 0.05% Tween 20) | 5% Donkey serum (Sigma – D9663) in PBS | Goat anti-GFP (1:200, Abcam – ab6673) overnight at 4°C | AF488 Donkey anti-goat (1:200, Jackson ImmunoResearch – 705-546-147), one hour at room temperature |
| CD31 (immune-histochemistry) | Boiling for 30 min in citric acid buffer (10 mM citric acid, pH 6.0, 0.05% Tween 20) | - 3% H2O2 solution (peroxidase inactivation) 30 min at room temperature;<br>- 10% Goat serum (Sigma – G9023) and 1% BSA in PBS | Rabbit anti-CD31 (1:50, Abcam – ab28364) overnight at 4°C | Goat anti-Rabbit IgG, biotinylated (1:1000, Abcam – ab6720), one hour at room temperature, then Streptavidin-horse radish peroxidase (1:250 Rockland S000-03), one hour at room temperature, then DAB (Dako – K3468), 3-20 minutes at room temperature |
| CD31 (immune- | Boiling for 30 min in citric acid buffer (10 mM citric acid, pH | 15% Donkey serum (Sigma – D9663) in PBS | Rabbit anti-CD31 (1:50, Abcam – | AF594 Donkey anti-rabbit (1:200, Jackson ImmunoResearch 711- |

| | | | | |
|---|---|---|---|---|
| fluorescence – assay 1) | 6.0, 0.05% Tween 20) | | ab28364) overnight at 4°C | 546-152), one hour at room temperature |
| CD31 (immune-fluorescence – assay 2) | Boiling for 20 min in Tris-EDTA buffer (10 mM Tris, 1 mM EDTA, 0.05% Tween 20, pH 9.0,) | Animal-free blocking solution (Vector – SP-5030) | Goat anti-CD31 (1:20, R&D – AF3628) overnight at 4°C | NL557-conjugated Donkey Anti-Goat (1:200, R&D – NL001), one hour at room temperature |
| F4/80 | Heat-induced antigen retrieval in Target Retrieval Solution (pH=6) – Dako S236984-2 | - Bloxall (peroxidase) Blocking Solution – Vector Labs SP-6000;<br>- Animal-Free Blocker - Vector Labs SP-5030 | Rat anti-Mouse F4/80 (1:20, [CI:A3-1] – Bio-Rad MCA497) 1 hour at room temperature | - Rabbit anti-Rat IgG (H+L) (1:250, Bethyl A110-322A) 1 hour at room temperature;<br>- Anti-Rabbit HRP (ImmPress – Vector Labs MP-7451) 30 min at room temperature;<br>- DAB (ImmPact DAB Kit - Vector Labs SK-4105) |
| MCT1 | Proteinase K digestion (Dako – S3020) for 3 minutes at room temperature | 15% Donkey serum (Sigma – D9663) in PBS | Chicken anti-MCT1 (1:200, Merk Millipore – AB1286-I) overnight at 4°C | AF488 Donkey anti-chicken (1:200, Jackson ImmunoResearch – 703-546-155), one hour at room temperature |
| MCT4 | Proteinase K digestion (Dako – S3020) for 3 minutes at room temperature | 15% Donkey serum (Sigma – D9663) in PBS | Rabbit anti-MCT4 (1:500, Merck Millipore – AB3314P) overnight at 4°C | AF488 Donkey anti-rabbit (1:200, Jackson ImmunoResearch – 711-546-152), one hour at room temperature |
| Laminin | Proteinase K digestion (Dako – S3020) for 3 minutes at room temperature | 15% Donkey serum (Sigma – D9663) in PBS | Rabbit anti-laminin (1:500, Dako – Z0097) overnight at 4°C | AF488 Donkey anti-rabbit (1:200, Jackson ImmunoResearch – 711-546-152), one hour at room temperature |

928

929

930 **Supplementary Table 7: Primers used for qRT-PCR**

| Gene | Forward primer | Reverse primer | Amplicon (bp) |
|---|---|---|---|
| *Igf2* | AGTCCGAGAGGGACGTGTCTA | CGGACTGTCTCCAGGTGTCAT | 102 |
| *Angpt1* | GAAGCAACTTCTCAACAGACA | TTCTTTGTGTTTTCCCTCCATT | 100 |
| *Angpt2* | CTTCTACCTCGCTGGTGAAGAG | GCTAAAATCACTTCCTGGTTGG | 106 |
| *Tek* | GGAGTGGAGTGAAGAACTAGG | GTGGAGTCAGTGATGTTGGAGA | 93 |
| *Adgre1* | TAGCTGCTCTTCTGATACCCTC | CCAACATTCATCTTGTCCCCTC | 145 |
| *Gcm1* | CCGCAAGATTTACCTGAGACC | GAATAAGCTTCAGGGGTCCATT | 98 |
| *Syna* | AGCCCTCTCTGGACAATATTCA | CAAGGTGGGAGAAGATATTTGG | 89 |
| *Synb* | CAGCTGACACCCTCATTAAACA | ATCCAGAAATGGGAATGAAGTG | 122 |
| *Slc16a1* | TCGCAGCTTCTTTCTGTAACAC | TCATAGTCAGAGCTGGGTTCAA | 102 |
| *Slc16a3* | TGCAGAAGCATTATCCAGATCTAC | GTATCGATTGAGCATGATGAGG | 99 |
| *Ly6e* | ACATGAGAGTCTTCCTGCCTGT | TTCTGATCGGTACATGAGAAGC | 91 |
| *Adamts1* | CAAAGGACAGGTGCAAGCTC | TTGCACACAGACAGAGGTAGAG | 119 |
| *Cxcl10* | CGTCATTTTCTGCCTCATCCTG | TGATTTCAAGCTTCCCTATGGC | 134 |
| *Thbs1* | ATGTACCCATCCAGAGCATCTT | GGTTCCAAAGACAAACCTCACA | 125 |
| *Edn1* | GACATCATCTGGGTCAACACTC | AAGTCTTTCAAGGAACGCTTGG | 86 |

| | | | |
|---|---|---|---|
| *Iigp1* | ATGATTTGCCCTCCAGCTTTAC | ACTGAATATTCCCTTTTCTCATCCT | 117 |
| *Cdkn1a* | GAACATCTCAGGGCCGAAAAC | CACTTCAGGGTTTTCTCTTGCA | 96 |
| *Hey2* | CTGCCAAGTTAGAAAAGGCTGA | CTCATGAAGTCTGTGGCAAGAG | 118 |
| *Igf1r* | GTTATCCACGACGATGAGTGC | AGTCACCGAATCGATGGTTTTC | 150 |
| *Igf2r* | GGAAGACACCAGAACCAGACA | TGACACTCATCCTCTGGAAGC | 103 |
| *Insr* | GAGAGGATGTGAGACGACGG | AGCAGTTCTCCAGCTCATGTAG | 149 |
| *Gapdh* | ACAACTCACTCAAGATTGTCAGCA | ATGGCATGGACTGTGGTCAT | 121 |
| *Sdha* | TTCCGTGTGGGGAGTGTATTG | ATTCTGCAGCTCCAGGGTCTC | 135 |
| *Pmm1* | ATCCGGGAGAAGTTTGTGGAA | GCTGTCTTCATCCAGGCTGTC | 144 |
| *Ppia* | AAGGGTTCCTCCTTTCACAGAA | GATGCCAGGACCTGTATGCTT | 146 |

931

932